

Note on Upwinding Constrained Transport Method for Ideal Magnetohydrodynamics ¹²

Shengtai Li

Theoretical Division, Los Alamos National Laboratory

ABSTRACT

We describe several upwinding constrained transport (UCT) methods in this paper and compare them with the flux-CT method (Balsara & Spicer 1999). The results show that the divergence-free reconstruction is an improvement only for low- β plasma, where the pressure positivity becomes a problem. The energy-fix or pressure correction approach destroys overall conservation and leads to wrong states for some low- β MHD flows. For other problems, the flux-CT with the standard reconstruction on cell-centered values works well. This paves a way to use the dimensional splitting MHD solver for multidimensional problems.

1. Introduction

Many astrophysics problems demands solutions of ideal magneto-hydrodynamics equations (MHD). There are many numerical techniques to solve MHD equations. In this paper, we consider a Godunov type of method. Godunov's method and its various derivatives have gained increasing popularity in solving the Euler equations of hydrodynamics (HD) due to their robustness and ability to achieve high resolution near discontinuities. Central to these methods is the exact or approximate solutions of the Riemann problem (Riemann solver). In the last decade, several Godunov methods for HD have been extended to MHD flow. These methods conservatively update the zone-averaged or grid-centered fluid and magnetic field states based on estimated advective fluxes of mass, momentum, energy and magnetic field at grid interfaces using solutions to the Riemann problem at each interface. MHD examples include Brio and Wu (Brio & Wu 1998), Zachary et al. (Zachary et al. 1994), Dai and Woodward (Dai & Woodward 1994, 1998), Powell (Powell 1994), Ryu and Jones (Ryu & Jones 1995), Roe and Balsara (Roe & Balsara 1996), and Balsara (Balsara 1998), etc..

The MHD flow has an implicit constraint $\nabla \cdot \mathbf{B} = 0$. The feature of upwinding schemes that use the cell-centered quantities to estimate fluxes at the cell interfaces makes enforcing

¹This research was performed under the auspices of the Department of Energy. It was supported by the Laboratory Directed Research and Development Program at Los Alamos.

²Los Alamos Report LA-UR-03-8925

the constraint non-trivial. There are several approaches to handle this problem. Powell et al. (Powell et al. 1999) used a scheme of Powell (Powell 1994) to add a source term that is proportional to $\nabla \cdot \mathbf{B}$ to the original set of MHD equations. By that way any local $\nabla \cdot \mathbf{B}$ that is created is convected away. This approach leads to the Riemann problem which has an eight-wave structure. Recently, Janhunen (Janhunen 2000) formulated various arguments to add the $\nabla \cdot \mathbf{B}$ related source term only to the induction equation, which restores the momentum and energy conservation. Yet another approach has been proposed by Dedner et al. (Dedner et al. 2002) to damp the divergence errors while convecting it away by adding diffusion to the hyperbolic convection of the $\nabla \cdot \mathbf{B}$. Toth (Tóth 2000) pointed out that the eight-wave formulation can lead to incorrect jump conditions across strong shocks in the numerical solutions.

The *projection method* proposed in (Brackbill & Barnes 1983) has been widely used by many authors (e.g., (Jiang & Wu 1999)). However, the projection involves the solution of a Poisson equation and also restricts the choice of boundary conditions. Another way to keep $\nabla \cdot \mathbf{B}$ exactly zero is to rewrite the MHD equations in terms of vector potential \mathbf{A} and define the magnetic field as $\mathbf{B} = \nabla \times \mathbf{A}$. A disadvantage of this approach is that the order of spatial derivatives increases by one, which reduces the order of accuracy by one (see (Evas& Hawley 1989) for more details).

The *constrained transport* (CT) method by Evans and Hawley (Evas& Hawley 1989) is another approach to keep $\nabla \cdot \mathbf{B}$ to the accuracy of machine round-off error. This approach has been combined with various shock-capturing schemes by many authors (DeVore 1991; Dai & Woodward 1998; Ryu et al. 1998; Balsara & Spicer 1999; Londrillo& Del Zanna 2000). The original CT method used a staggered grid which places the magnetic field variables in the face center and the rest in the cell-center. The divergence-free finite-difference scheme can be easily constructed for the staggered grid (see Yee (Yee 1966)). Toth (Tóth 2000) introduced a finite-volume interpretation of the CT schemes that place all of the variables at the cell center. However, this idea is difficult to apply to an adaptive mesh refinement mesh. In this paper, we adopted a CT approach, which is similar to the one of (Balsara & Spicer 1999), implemented on the staggered grid. As in Toth (Tóth 2000), we called it *flux-CT* approach.

As other CT methods, the key step in flux-CT method is to evaluate the electro-motive-force (EMF, defined via $\mathbf{E} = \mathbf{v} \times \mathbf{B}$) at the nodes for 2D or at the edge-centers for 3D problems. The flux-CT method of (Balsara & Spicer 1999) exploited the duality between the upwind fluxes of the Godunov scheme and EMF in a plasma, and obtained the EMF via averaging the available related upwind fluxes. It can be easily implemented in any Godunov scheme. Toth (Tóth 2000) found the flux-CT was one of the most accurate second order schemes that he tested.

Balsara (Balsara 2003) raised four issues regarding to the improvement of the flux-CT scheme of (Balsara & Spicer 1999) and proposed some numerical schemes to solve it. First

the volume averaging cell-centered magnetic fields can be obtained uniquely by using the face-averaging face-centered magnetic fields. The simple arithmetic averaging is not optimal. Second, the divergence-free reconstruction of (Balsara 2000) can be used to evaluate the face-centered magnetic field components directly without using the limited cell-centered magnetic fields. Third, the continuity of the normal component of the magnetic field at cell-interface can be preserved by using the divergence-free reconstruction of (Balsara 2000), and hence eliminate the jump in the normal component and the need for the eight wave model of (Powell 1994). Finally, The EMF at the edge center (or nodes for 2D) can be evaluated directly at that point without averaging procedure. This is achieved by introducing more quadrature points located at the edge center and solving more Riemann problems.

These four issues also pertain to other CT schemes. A similar scheme, called *upwinding constrained transport* (UCT), was proposed in (Londrillo & Del Zanna 2003). UCT used a similar reconstruction to (Balsara 2000) to preserve the divergence-free condition of the face-centered values and evaluate the EMF upwindly and directly by using a four-state Riemann solver.

We will discuss and compare the numerical schemes of (Balsara 2003) and (Londrillo & Del Zanna 2003) in this paper. The outline is as follows. In Section 2, we review the schemes of (Balsara 2003) and (Londrillo & Del Zanna 2003). In Section 3 we unify the schemes and propose the implementations for our MHD solver. In Section 4, several examples are given to compare the modified schemes with the original flux-CT scheme of (Balsara & Spicer 1999).

2. Upwinding Constrained Transport Method

For the sake of simplicity, we will restrict our discussion for a two-dimensional uniform Cartesian grid with slab symmetry in the 3rd direction. B_x and B_y are face-centered values and satisfy the divergence-free condition. All of the other components are cell-centered values and updated by the Godunov scheme. Generalization to 3D is quite trivial. For the sake of clarity, the cell-centered representation of the magnetic field will be denoted by capital \mathbf{B} , while the face-centered representation by lower case \mathbf{b} in the difference formula.

2.1. Flux-CT

We first describe the constrained transport method and the flux-CT scheme of (Balsara & Spicer 1999). The CT method by Evans and Hawley (Evas& Hawley 1989) applied a staggered grid to maintain the divergence-free constraint for finite-difference schemes. The magnetic fields are represented on the cell interfaces. In 2D, the b_x and b_y are shown in Fig.2.1. The main idea of the CT scheme is to place the electric field E at the nodes. The

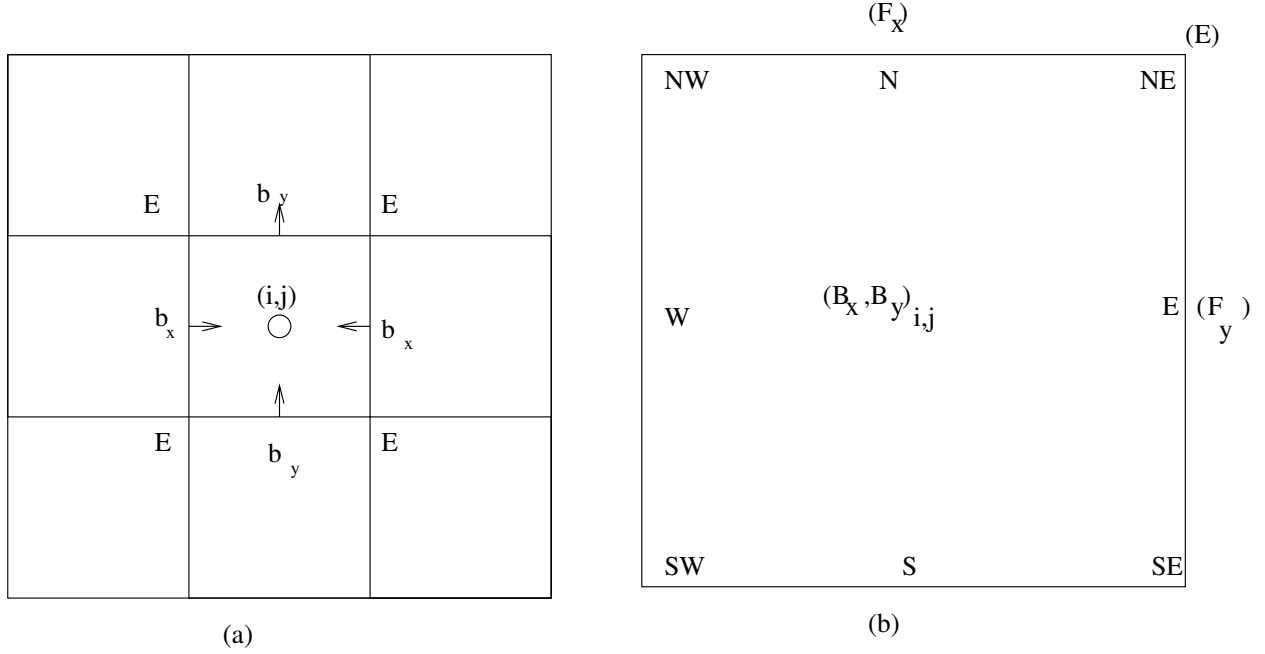


Fig. 2.1.— (a) Staggered grid and constrained transport in 2D. The interface centered fields b_x and b_y are advanced by finite differencing of the electric field E located at the nodes. (b) The notation used for the reconstruction inside the cell. Fluxes are either defined as two-state functions located at cell-interfaces or a four-state function located at the nodes.

induction equation is then discretized by Yee’s method (Yee 1966) as

$$\begin{aligned}
 b_{x,i+\frac{1}{2},j}^{n+1} &= b_{x,i+\frac{1}{2},j}^n - \Delta t \frac{E_{i+\frac{1}{2},j+\frac{1}{2}} - E_{i+\frac{1}{2},j-\frac{1}{2}}}{\Delta y}, \\
 b_{y,i,j+\frac{1}{2}}^{n+1} &= b_{y,i,j+\frac{1}{2}}^n + \Delta t \frac{E_{i+\frac{1}{2},j+\frac{1}{2}} - E_{i-\frac{1}{2},j+\frac{1}{2}}}{\Delta x}.
 \end{aligned} \tag{1}$$

It is easy to verify that the numerical divergence of \mathbf{b} at the cell-center, defined by

$$(\nabla \cdot \mathbf{b})_{i,j} = \frac{(b_x)_{i+\frac{1}{2},j} - (b_x)_{i-\frac{1}{2},j}}{\Delta x} + \frac{(b_y)_{i,j+\frac{1}{2}} - (b_y)_{i,j-\frac{1}{2}}}{\Delta y}$$

is preserved during the time integration. Therefore, if $\nabla \cdot \mathbf{b} = 0$ holds initially, it holds forever to the accuracy of round-off errors.

Many CT schemes have been proposed (see (DeVore 1991; Dai & Woodward 1998; Ryu et al. 1998; Balsara & Spicer 1999; Londrillo & Del Zanna 2000)). The main difference between them is how to obtain the EMF E . Toth (Tóth 2000) has compared several CT schemes and found the flux-CT of (Balsara & Spicer 1999) is one of the most accurate. In (Balsara & Spicer 1999), Balsara and Spicer combined the CT approach with an arbitrary Godunov type base scheme by interpolating appropriately the signed cell-interface upwind

fluxes F^x and F^y into the EMF at the node,

$$E_{i+\frac{1}{2},j+\frac{1}{2}} = \frac{1}{4}(-F_{i+\frac{1}{2},j}^x - F_{i+\frac{1}{2},j+1}^x + F_{i,j+\frac{1}{2}}^y + F_{i+1,j+\frac{1}{2}}^y). \quad (2)$$

Since all of the four fluxes have been available in the upwind step of a Godunov-scheme, the flux-CT is easy to implement without involving much extra computation.

In (Balsara & Spicer 1999), Balsara and Spicer also described a variant of their scheme, which used an upwind interpolation for (2) in the vicinity of magneto-sonic shocks according to the direction of the local pressure gradient, which is

$$E_{i+\frac{1}{2},j+\frac{1}{2}} = 0.5\psi(-F_{i+\frac{1}{2},j}^x - F_{i+\frac{1}{2},j+1}^x) + 0.5(1 - \psi)(F_{i,j+\frac{1}{2}}^y + F_{i+1,j+\frac{1}{2}}^y), \quad (3)$$

where $\psi = \Delta P_x / (\Delta P_x + \Delta P_y)$ is a ratio between the gradient in x -direction and total gradient. By this variant, the 2D scheme can be reduced to 1-D scheme near the shock if the shock aligns with one of the coordinate axes. However, it does not have significant improvement for other cases (Balsara & Spicer 1999).

Flux-CT works quite well for many problems (see (Balsara & Spicer 1999; Tóth 2000)). However, it can cause negative pressure for a low- β ($\beta = 2p/(\mathbf{B}^2)$) MHD flow. Similar to the energy fix for the projection method, Balsara and Spicer (Balsara & Spicer 1999) proposed a fix to correct the energy density for the new magnetic field. That is, if \mathbf{B}_c^{n+1} is the cell-centered value obtained by advancing the field directly using the high order Godunov scheme, and \mathbf{B}_{fc}^{n+1} is the new cell-centered values obtained by averaging the face-centered values \mathbf{b}^{n+1} to the cell-center, then the energy density is corrected as

$$e_{new} = e_{old} + \frac{1}{2} ((\mathbf{B}_{fc}^{n+1})^2 - (\mathbf{B}_c^{n+1})^2). \quad (4)$$

As pointed out in (Balsara & Spicer 1999), this step is an optional step. It results in a slight loss of total energy conservation at the level of discretization error. Many real work applications and test problems (see (Balsara & Spicer 1999; Tóth 2000)) do not need this step. However, it proves to be useful to maintain a positive pressure for a low- β MHD flow. In Section 4, we will find out that the deviation of the numerical solution from the true solutions depends highly on the difference between the numerical e_{new} and the conservative energy. Eq. (4) should be used cautiously.

Although the divergence-free condition is preserved after each CT step, the numerical monopoles are still produced in the upwind step of the Godunov method. This is because the upwind reconstruction is based on the cell-centered values of the magnetic field, which is usually obtained via the arithmetic averaging by many practitioners (see (Dai & Woodward 1998; Ryu et al. 1998; Balsara & Spicer 1999)),

$$B_{x,i,j} = \frac{1}{2}(b_{x,i-\frac{1}{2},j} + b_{x,i+\frac{1}{2},j}), \quad (5)$$

$$B_{y,i,j} = \frac{1}{2}(b_{y,i,j-\frac{1}{2}} + b_{y,i,j+\frac{1}{2}}). \quad (6)$$

Also, the normal component of the magnetic field obtained from the reconstruction may be not continuous at the cell interfaces in each direction for a multidimensional problem, which means that the eight-wave model of (Powell 1994) might be needed.

In this paper, we use the flux-CT as our basic CT scheme. We will test its several variants, including the energy fix (4).

2.2. Modified Flux-CT

The modified flux-CT was proposed in (Balsara 2003). First, The cell-interface values of the magnetic field is evaluated directly from the divergence-free monotonicity preserving reconstruction of the face-centered values of \mathbf{b} . The reconstruction polynomial for the 2D Cartesian grid is

$$b_x(x, y) = a_0 + a_x x + a_y y + a_{xx} x^2 + a_{xy} xy + a_{yy} y^2, \quad (7)$$

$$b_y(x, y) = c_0 + c_x x + c_y y + c_{xx} x^2 + c_{xy} xy + c_{yy} y^2, \quad (8)$$

where the coefficients are defined by

$$a_y = \frac{1}{2}(\Delta_y b_x^+ + \Delta_y b_x^-), \quad (9)$$

$$c_x = \frac{1}{2}(\Delta_x b_y^+ + \Delta_x b_y^-), \quad (10)$$

$$a_{xy} = -2c_{yy} = \frac{\Delta_y b_x^+ - \Delta_y b_x^-}{\Delta x}, \quad (11)$$

$$c_{xy} = -2a_{xx} = \frac{\Delta_x b_y^+ - \Delta_x b_y^-}{\Delta y}, \quad (12)$$

$$a_0 = \frac{b_x^+ + b_x^-}{2} - a_{xx} \frac{\Delta^2 x}{4}, \quad (13)$$

$$c_0 = \frac{b_y^+ + b_y^-}{2} - c_{yy} \frac{\Delta^2 y}{4}, \quad (14)$$

where $\Delta_y b_x$ and $\Delta_x b_y$ are the limited slope of b_x along the y -direction and b_y along the x -direction at the cell-interfaces, b^+ represents the value at the right or top face and b^- represents the value at the left or bottom face. We should point out that although (7) and (8) are quadrature polynomials, the reconstruction is of only the second order accuracy.

A direct integration of (7) and (8) over the whole cell yields the cell-centered volume-averaging value of \mathbf{b} , which is

$$B_x = \frac{b_x^+ + b_x^-}{2} - a_{xx} \frac{\Delta^2 x}{6} \quad (15)$$

$$B_y = \frac{b_y^+ + b_y^-}{2} - c_{yy} \frac{\Delta^2 y}{6} \quad (16)$$

It is clear that for a second order scheme, the second term in B_x and B_y can be neglected, by which the (15) and (16) are reduced to Eqs. (5) and (6).

Balsara pointed out in (Balsara 2003) that the (15) and (16) are important in maintaining a positive pressure for strong shocks moving through low- β plasmas. However, we will find out in Section 4 that this may not be true for our MHD solvers. The energy fix (4) is more important and necessary than the (15) and (16) in those cases.

The divergence-free reconstruction is designed so that the interpolation polynomials $b_x(x, y)$ and $b_y(x, y)$ naturally match b_x and b_y at the cell-interfaces. Therefore, the divergence-free condition of the cell-interface values is automatically preserved, and the normal component of the magnetic fields is continuous at the cell-interfaces. No eight-wave model of (Powell 1994) is needed.

The limiters are applied directly to the face-centered values in the reconstruction $b_x(x, y)$ and $b_y(x, y)$. Several limiting strategies have been proposed in (Balsara 2003). In the numerical tests of Section 4, we adopt a fast TVD limiting (Balsara 2003), which is defined by

$$\Delta_y b_{x,\cdot,j} = \text{Limiter} \left(\frac{b_{x,\cdot,j+1} - b_{x,\cdot,j}}{\Delta y}, \frac{b_{x,\cdot,j} - b_{x,\cdot,j-1}}{\Delta y} \right) \quad (17)$$

$$\Delta_x b_{y,i,\cdot} = \text{Limiter} \left(\frac{b_{y,i+1,\cdot} - b_{y,i,\cdot}}{\Delta x}, \frac{b_{y,i,\cdot} - b_{y,i-1,\cdot}}{\Delta x} \right), \quad (18)$$

where limiter represents one of the minmod, monotonic-central, or van Leer limiter.

The original flux-CT method calculated the EMF via spatial averaging in (2). Balsara (Balsara 2003) proposed yet another approach to evaluate the flux (EMF) directly at the nodes of the grid. Consider the EMF at node $(x_{i+\frac{1}{2}}, y_{j+\frac{1}{2}})$. We can obtain four states at the node from the reconstruction of the cell-centered values located at (x_i, y_j) , (x_{i+1}, y_j) , (x_{i+1}, y_{j+1}) and (x_i, y_{j+1}) . Four Riemann problems are solved to obtain the flux at the specific node. Since the flux is evaluated at the node, no spatial interpolation is needed to obtain the EMF. Note that more Riemann problems need to be solved (about twice as many as that of the original face interface-centered approach). It is debatable if this more computational effort is worth for the accuracy it obtains. In Section 4, we will see that for a second order method, more Riemann problems solved do not mean more accuracy gained.

2.3. Upwind Constrained Transport

Londrillo and Del Zanna recently proposed a similar approach to advance the magnetic fields, which is called *upwind constrained transport* (UCT) method.

The reconstruction of the magnetic field uses the cell-centered values and is the same as for other cell-centered components, except that the slopes of the magnetic field in the

normal direction of the interfaces are calculated differently. The implementation of UCT is as follows. First the cell-centered magnetic fields are obtained via arithmetic averaging. Then the reconstruction for the cell-centered values is obtained as

$$B_x(x, y) = B_x + \Delta_x(b_x)(x - x_j) + \Delta_y(B_x)(y - y_j), \quad (19)$$

$$B_y(x, y) = B_y + \Delta_x(B_y)(x - x_j) + \Delta_y(b_y)(y - y_j), \quad (20)$$

where $\Delta_y(B_x)$ and $\Delta_x(B_y)$ are the limited slopes of \mathbf{B} field, $\Delta_x(b_x)$ and $\Delta_y(b_y)$ are obtained directly by central differencing of \mathbf{b} field at the cell-center. It can be easily verified that the divergence-free condition

$$\Delta_x(b_x) + \Delta_y(b_y) = 0$$

is preserved by the reconstruction.

In the upwind step, the cell-centered components are advanced by the Godunov scheme. The numerical flux is usually obtained by a Riemann solver. Suppose the left and right states of the Riemann problem is U_R and U_L , then the numerical flux can be written as

$$F(U_R, U_L) = \frac{1}{2}(F(U_R) + F(U_L)) - \phi,$$

where the first term expressing the smooth component leads to a centered two-point formula in flux differentiation and the second is a dissipation term coming from the upwind procedure.

The face-centered components (magnetic fields) are advanced with the staggered method. The EMF is evaluated by a linear combination of 1-D upwind fluxes along the intersecting direction, since a same flux component at the same collocation point results to have two independent representations in terms of characteristic wave fans. The EMF at each node can be evaluated as a four-state flux function (see Fig.2.1). To preserve the continuity and upwind properties along each direction, EMF is constructed as

$$E(U^E, U^W, U^S, U^N) = E_{\text{avg}} - \phi_y + \phi_x, \quad (21)$$

where the first term expressing the smooth part can be evaluated by a centered four-point formula, e.g.,

$$E_{\text{avg}} = \frac{1}{4}(E^{NE} + E^{SE} + E^{NW} + E^{SW}),$$

the second term coming from the upwind procedure of the Riemann solver can be evaluated by spatial averaging,

$$\phi_x = \frac{1}{2}(\phi_x^N + \phi_x^S), \quad \phi_y = \frac{1}{2}(\phi_y^E + \phi_y^W).$$

Londrillo and Del Zanna (Londrillo & Del Zanna 2003) proposed two schemes with respect to two Riemann solvers to evaluate $E(U^E, U^W, U^S, U^N)$ efficiently. In the first based on Roe's type scheme, the smooth term can be evaluated as

$$(E_{\text{avg}})_{i+\frac{1}{2}, j+\frac{1}{2}} = -\frac{1}{2}[(\hat{v}_x b_y)_{i+1} + (\hat{v}_x b_y)_i]_{j+\frac{1}{2}} + \frac{1}{2}[(\hat{v}_y b_x)_{j+1} + (\hat{v}_y b_x)_j]_{i+\frac{1}{2}}, \quad (22)$$

where $(\hat{v}_x)_{i,j+\frac{1}{2}} = \frac{1}{2}[(v_x)_j + (v_x)_{j+1}]_i$, and $(\hat{v}_y)_{i-\frac{1}{2},j} = \frac{1}{2}[(v_y)_i + (v_y)_{i+1}]_j$. The dissipative terms can be evaluated as a two-point average,

$$\begin{aligned}(\phi_x)_{i+\frac{1}{2},j+\frac{1}{2}} &= \frac{1}{2}[(\phi_x)_j + (\phi_x)_{j+1}]_{i+\frac{1}{2}}, \\(\phi_y)_{i+\frac{1}{2},j+\frac{1}{2}} &= \frac{1}{2}[(\phi_y)_i + (\phi_y)_{i+1}]_{j+\frac{1}{2}}.\end{aligned}\tag{23}$$

Since the four contributes of ϕ are already obtained from the Riemann solver, (23) can be easily implemented.

The second scheme are based on the HLLC Riemann solver, or so-called central-type schemes. The smooth term is evaluated as

$$E_{\text{avg}} = \frac{\alpha_x^+ \alpha_y^+ E^{NE} + \alpha_x^+ \alpha_y^- E^{SE} + \alpha_x^- \alpha_y^+ E^{NW} + \alpha_x^- \alpha_y^- E^{SW}}{(\alpha_x^+ + \alpha_x^-)(\alpha_y^+ + \alpha_y^-)},\tag{24}$$

and the dissipative terms are evaluated as

$$\phi_x = \frac{\alpha_x^+ \alpha_x^-}{\alpha_x^+ + \alpha_x^-} (b_y^W - b_y^E), \quad \phi_y = \frac{\alpha_y^+ \alpha_y^-}{\alpha_y^+ + \alpha_y^-} (b_x^S - b_x^N)\tag{25}$$

where the α_x^\pm and α_y^\pm are the maximum characteristic speeds among the four reconstructed states at the node. For LLF fluxes, $\alpha_x^+ = \alpha_x^- = \alpha_x$ and $\alpha_y^+ = \alpha_y^- = \alpha_y$, the scheme can be reduced to

$$\begin{aligned}E_{\text{avg}} &= \frac{1}{4}(E^{NE} + E^{SE} + E^{NW} + E^{SW}), \\ \phi_x &= \frac{1}{2}\alpha_x(b_y^W - b_y^E), \\ \phi_y &= \frac{1}{2}\alpha_y(b_x^S - b_x^N),\end{aligned}\tag{26}$$

$$\tag{27}$$

3. General UCT Scheme and its Variation

The above described schemes can be unified and characterized by using control parameters. The main difference of the different CT schemes is on the evaluation of EMF. As mentioned in Section 2.3, we can write the EMF into two parts: smooth and dissipative part, which is

$$E(U^E, U^W, U^S, U^N) = E_{\text{avg}} - \phi_E = E_{\text{avg}} - c_\phi \cdot (\phi_y - \phi_x),\tag{28}$$

where c_ϕ is a constant coefficient.

There are several ways to evaluate the smooth part E_{avg} . The transport flux-CT method of Ryu et al. (Ryu et al. 1998) evaluated it as a spatial averaging over four cell-centered points, which is

$$(E_{\text{avg}})_{i+\frac{1}{2},j+\frac{1}{2}} = \frac{1}{4}(E_{i,j} + E_{i,j+1} + E_{i+1,j} + E_{i+1,j+1}).\tag{29}$$

The original flux-CT scheme of (Balsara & Spicer 1999) evaluated it as a spatial averaging over eight values obtained at the cell-interfaces, which is

$$(E_{\text{avg}})_{i+\frac{1}{2},j+\frac{1}{2}} = \frac{1}{8} (E_{i,j+\frac{1}{2}}^+ + E_{i,j+\frac{1}{2}}^- + E_{i+1,j+\frac{1}{2}}^+ + E_{i+1,j+\frac{1}{2}}^- + E_{i+\frac{1}{2},j}^+ + E_{i+\frac{1}{2},j}^- + E_{i+\frac{1}{2},j+1}^+ + E_{i+\frac{1}{2},j+1}^-). \quad (30)$$

It is clear that (30) and (29) are identical if a piecewise-constant reconstruction is used. Londrillo and Del Zanna (Londrillo & Del Zanna 2003) evaluated E_{avg} as a two-part combination in Eq.(22) and as an average state over the Riemann fan in Eq. (24). Balsara (Balsara 2003) evaluated it as an averaging over four possible values at the nodes, which is

$$(E_{\text{avg}})_{i+\frac{1}{2},j+\frac{1}{2}} = \frac{1}{4} [E(U_{i+\frac{1}{2},j+\frac{1}{2}}^{SE}) + E(U_{i+\frac{1}{2},j+\frac{1}{2}}^{SW}) + E(U_{i+\frac{1}{2},j+\frac{1}{2}}^{NE}) + E(U_{i+\frac{1}{2},j+\frac{1}{2}}^{NW})], \quad (31)$$

where $U_{i+\frac{1}{2},j+\frac{1}{2}}^{a,b}$ with $a = N, S, b = E, W$ are obtained through the reconstruction.

In term of the computational effort for a general second-order Godunov scheme, (30) is readily available from the Riemann solver at the cell-interfaces. However, (29), (22) and (31) need some extra computation to evaluate E at some specific points. (31) requires the most computation because it also needs the reconstruction at the cell-corner from four cell-centered values.

Different schemes evaluated the second term ϕ_E of (28) differently. It can be either obtained from the Riemann solver or evaluated directly via (25) or (27). One of the big differences is in the coefficient c_ϕ . If the fluxes are obtained at the center of face-interfaces, ϕ_E is evaluated as

$$\phi_E = c_\phi (\phi_y^W + \phi_y^E - \phi_x^S - \phi_x^N). \quad (32)$$

In (Balsara & Spicer 1999), $c_\phi = 0.25$, Eq.(32) becomes

$$\phi_E = \frac{1}{4} (\phi_y^W + \phi_y^E - \phi_x^S - \phi_x^N). \quad (33)$$

In Ryu et al. (Ryu et al. 1998) and Londrillo and Del Zanna (Londrillo & Del Zanna 2003), $c_\phi = 0.5$, Eq.(32) becomes

$$\phi_E = \frac{1}{2} (\phi_y^W + \phi_y^E - \phi_x^S - \phi_x^N). \quad (34)$$

As we can see, there is a factor of 2 difference between different c_ϕ s. The scheme (34) has a nice property that it reduces to the correct 1-D flux for problems aligned with one of the coordinate axes or diagonals. This property does not hold for (33). However, as we will see from the numerical results in section 4, the excessive dissipation of (34) may not be good for a general 2D problem.

If the fluxes are obtained at the corners of the cells, ϕ_E is evaluated as

$$\phi_E = c_\phi (\phi_y^{NW} + \phi_y^{NE} - \phi_x^{SW} - \phi_x^{SE}). \quad (35)$$

The modified flux-CT method (Balsara 2003) uses $c_\phi = 1/4$.

4. Numerical Experiment

In this section, we compared the divergence-free reconstructions and several UCT schemes with the original flux-CT method. One of the disadvantages of the divergence-free reconstruction is that it cannot be used in a dimensional splitting solver. This is because at each intermediate stage in a time step, the divergence-free condition may not be held and it is also impossible to use the Yee’s method to the face-centered magnetic field at each intermediate stage. Therefore, an unsplit version of our MHD code is used. Our code has been described in details in (Li & Li 2003). It contains several Riemann solvers (HLL, HLLC, Roe’s and Hybrid) and several reconstructions, which includes the divergence-free reconstructions of (Balsara 2003) and (Londrillo & Del Zanna 2003). To have a consistent comparison, we use the van Leer limiter whenever the limiter is needed during the reconstruction.

The main computational steps of our unsplit MHD solver consist of: a reconstruction procedure based on the primitive variables, a Riemann solver to calculate the flux at the cell-interfaces, a spatial averaging to calculate the EMF at the cell-corners, and a second-order Runge-Kutta time integration.

We want to compare two things. First how different divergence-free reconstructions affect the numerical results. As we have mentioned the divergence-free reconstruction has two advantages: it removes the numerical monopole in the Riemann-solver and it removes the jump of the magnetic field at the cell-interface in the normal direction and eliminates the need of the eight-wave model of (Powell 1994). However, one of the disadvantages is that the slope of the magnetic field is not limited along the normal direction and may introduce oscillations.

Since the divergence-free reconstruction (7) and (8) leads to the volume-average magnetic field at the cell-center. We want to know how the volume-average magnetic field at the cell-centered affect the numerical results. Does it preserve the pressure positivity without the energy-fix step?

Secondly, we we want to compare different UCT schemes: different smooth term evaluation combined with different dissipative term evaluations.

The time step is determined adaptively according to the current wave speed and CFL number. Without specification, CFL=0.7 is used. The computation is done on our Linux PC with 1.7GHz AMD Athlon processor. Whenever the parallel computation is needed, it is done on a four-processor cluster with 1.2GHz AMD Athlon processor.

4.1. Rotated shock-tube problems

These test problems involve the propagation of discontinuities defined by usual 1-D shock-tubes on a 2-D computational plane, and have been tested by many authors (see (Brio & Wu 1998; Ryu & Jones 1995; Balsara 1998; Tóth 2000; Falle 2002; Londrillo & Del Zanna 2003) for more details). The initial left and right states of the four shock-tube problems considered here are listed in Table 1. The first shock-tube problem ST-1 is a coplanar 2D

Table 1: Initial left (L) and right (R) states for the rotated shock tube problem

	ρ	v_{\parallel}	v_{\perp}	v_z	p	B_{\parallel}	B_{\perp}	B_z
Test ST-1: L	1	10	0	0	20	$5/\sqrt{4\pi}$	$5/\sqrt{4\pi}$	0
Test ST-1: R	1	-10	0	0	1	$5/\sqrt{4\pi}$	$5/\sqrt{4\pi}$	0
Test ST-2: L	1.08	1.2	0.01	0.5	0.95	$2/\sqrt{4\pi}$	$3.6/\sqrt{4\pi}$	$2/\sqrt{4\pi}$
Test ST-2: R	1	0	0	0	1	$2/\sqrt{4\pi}$	$4/\sqrt{4\pi}$	$2/\sqrt{4\pi}$
Test ST-3: L	1	0	0	0	1	0.75	1	0
Test ST-3: R	0.125	0	0	0	0.1	0.75	-1	0
Test ST-4: L	0.5	0	2	0	10	$2/\sqrt{4\pi}$	$2.5/\sqrt{4\pi}$	0
Test ST-4: R	0.1	-10	0	0	0.1	$2/\sqrt{4\pi}$	$2/\sqrt{4\pi}$	0

problem with an initially uniform magnetized background. The second problem ST-2 is a 2.5D problem with nonzero b_z and v_z which involving Alfvénic wave propagation. The third one ST-3 is a Riemann problem contains a slow compound structure. The fourth one ST-4 is a coplanar Riemann problem with a relatively low- β ($\beta = 0.16$ behind the fast shock).

We have tested these problems with different angles between shock interface and the y -axes. $\alpha = 45^\circ$ and $\alpha = \tan^{-1} 2 \approx 63.4^\circ$ are used. The final times t_{\max} are 0.08, 0.2, 0.1, and 0.06 respectively. For an angle α , the final time becomes $t_{\max} \cos(\alpha)$. As suggested by Toth (Tóth 2000), the computational domain for the rotated shock-tube tests may be reduced to a narrow strip $N \times 2$ grid. Periodic shifted boundary conditions in y -direction are applied. In our tests, $N = 400$ is used, which is compared with a reference solution computed with $N = 1600$ and $\alpha = 0$.

To quantify the numerical error, we calculate an L1 error as follows. First we obtain a reference solution of 400 nodes by averaging the solutions of $N = 1600$ over each coarse cell. Then the difference between the numerical solutions and reference solutions is calculated. Finally, the error is calculated as

$$Err = \sum_{i=1}^{N_u} \sum_{j=1}^N \frac{|\Delta u_j^i|}{\max_j |u^i|}, \tag{36}$$

where u^i is only for the cell-centered variables.

Since the CT method can preserve the divergence of the magnetic field, it is important to set the initial magnetic field to be divergence-free. ST-1 has a constant \mathbf{b} field initially and hence for any locally spacing of Δx and Δy , the divergence-free condition is satisfied. For the other three problems, there is a jump in B_y field. The easiest way to set up an initial divergence-free magnetic field is to align the shock interface along the diagonals of the cell, which is equivalent to have $\Delta x = \tan \alpha \Delta y$. We have verified that when $\Delta x = \tan \alpha \Delta y$ is satisfied, both the $\nabla \cdot B = 0$ and $B_{\parallel} = \text{constant}$ hold within machine accuracy.

For general grid spacing and α , we can first obtain the potential field A at each node from the given value of magnetic field B_{\parallel} and B_{\perp} , and then obtain the B_x and B_y at the cell-interfaces via the central differencing of A . In this approach, A must be defined in a way that it has unique value at each node no matter which integration path is used. For $\alpha = \tan^{-1} 2$ and $\Delta x = \Delta y$, we used another simple approach, which is illustrated in Fig.4.2. We can see that B_x^L, B_x^R, B_y^L , and B_y^R can be obtained directly from the constant states of

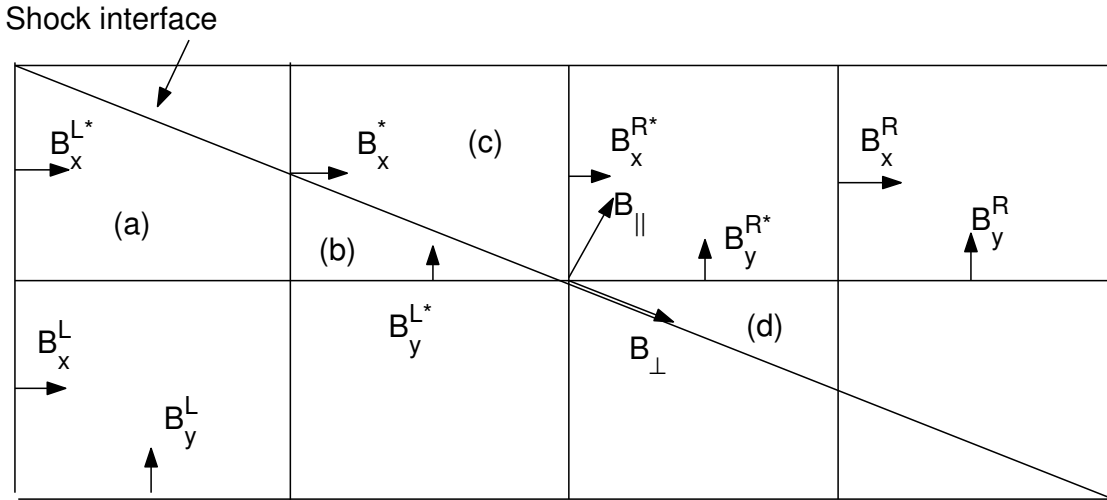


Fig. 4.2.— Initial magnetic field for oblique shock-tube problem with $\alpha = \tan^{-1} 2$ and $\Delta x = \Delta y$. (a) and (c) are quadrilaterals with an edge shared with the shock interface. (b) and (d) are triangles with an edge shared with the shock interface.

B_{\parallel} and B_{\perp} . B_x^* can be defined as $B_x^* = \frac{1}{2}(B_x^L + B_x^R)$. The other quantities ($B_x^{L*}, B_x^{R*}, B_y^{L*}$, and B_y^{R*}) can be calculated by the divergence-free condition in each quadrilateral or triangle, which yields

$$\begin{aligned} B_x^{L*} &= \frac{B_{\parallel}}{\sin \alpha} + \frac{1}{2} B_x^L - B_y^L, \\ B_x^{R*} &= \frac{B_{\parallel}}{\sin \alpha} + \frac{1}{2} B_x^R - B_y^R, \\ B_y^{L*} &= \frac{B_{\parallel}}{\sin \alpha} - \frac{1}{2} B_x^L, \end{aligned}$$

$$B_y^{R*} = \frac{B_{\parallel}}{\sin \alpha} - \frac{1}{2} B_x^R.$$

The magnetic field at other positions can be obtained by the continuity along the traverse direction $\eta = y \cos \alpha - x \sin \alpha$. It can be verified easily that the $\nabla \cdot \mathbf{b} = 0$ in each local cell. We should point out that although $\nabla \cdot \mathbf{b} = 0$ holds within machine round-off error, the conservation of the B_{\parallel} is accurate only to truncation errors at best (see Tóth (2000)).

4.1.1. Tests for different reconstructions

We first test these problems by using the flux-CT scheme (Balsara & Spicer 1999) with different reconstructions on the magnetic fields. The first, which we denote as BS, is the reconstruction based on cell-centered value of \mathbf{B} with limited slopes in both x and y direction. \mathbf{B} is calculated by arithmetic averaging. The second, denoted as BS2, is the reconstruction based on \mathbf{B} but with different slopes in normal direction. (19) and (20) will be used and the cell-centered values are calculated by arithmetic averaging. The third one, denoted as BS3, is a fully divergence-free reconstruction based on face-interface value of \mathbf{b} (Balsara 2000), where (7) and (8) are used. BS3 also implies that the volume-averaging values of the cell-centered \mathbf{B} , defined by (15) and (16), are used in the reconstruction.

Fig.4.1 shows the results for ST-1. In order to see the difference between these reconstructions, Only a “zoomed” part from a whole plot is shown. The plots for other shock-tube problems are also zoomed. We should point out that although the results for the angle $\alpha = \tan^{-1} 2$ and $\Delta y = 0.5 \Delta x$ are not shown here, they are almost the same as those in Fig.4.1. This feature, which is also shared by other shock-tube problems, means that it does not matter much how oblique the shock is as long as the parallel-component of the magnetic field is preserved. The results shows that BS3 is more dissipative near the slow rarefaction, slow shock, and the contact discontinuity. The results of BS2 coincide with those of BS very well. The numerical error w.r.t. the reference solutions is listed in Table 2.

The results for ST-1 with $\alpha = 63.4^\circ$ and $\Delta y = \Delta x$ are shown in Fig.4.2. B_{\parallel} has some errors around the true solution and the slow rarefaction is poorly resolved. It is interesting to note that the three reconstructions gave almost the same results.

Figs.4.3 and 4.4 show the results for ST-2. For both angles, the three reconstructions gave almost the same results. Figs.4.5 and 4.6 show the results for ST-3. From Fig.4.5, we see again that the BS3 is more dissipative than BS and BS2. It reflects on the resolution of compound structure and fast rarefaction. Both BS and BS2 have overshoot at the rarefaction (see the plot of v_{\parallel} in Fig.4.5) which BS3 does not have. As regards to the slow compound, for both angles, the BS is the best among the three reconstructions. We see oscillations for BS2 and BS3 scheme. BS3 has larger error than both BS and BS2 schemes. The oscillations might be due to the unlimited slope of the magnetic fields in the normal direction.

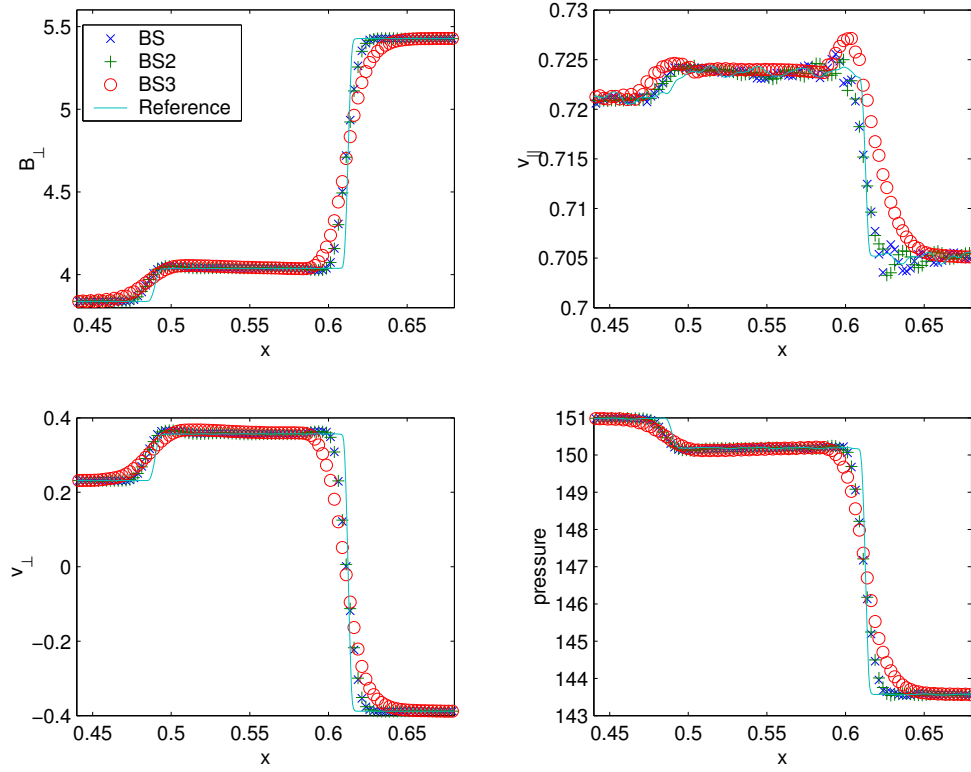


Fig. 4.1.— Results for shock-tube problem ST-1. Only a “zoomed” part from a whole plot is shown. The angle between the shock interface and y -axis is $\alpha = 45$. Output is at $t = 0.08/\sqrt{2}$.

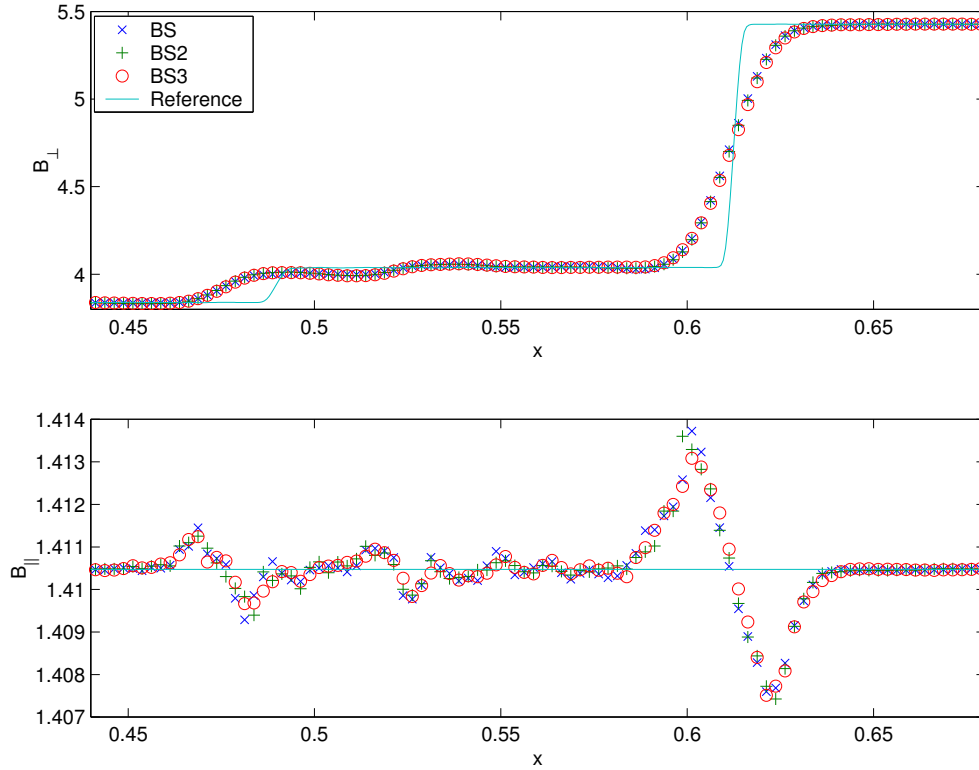


Fig. 4.2.— Results for shock-tube problem ST-1. Only a “zoomed” part from a whole plot is shown. $\alpha = \tan^{-1} 2$. $\Delta x = \Delta y$. Output is at $t = 0.08/\sqrt{5}$.

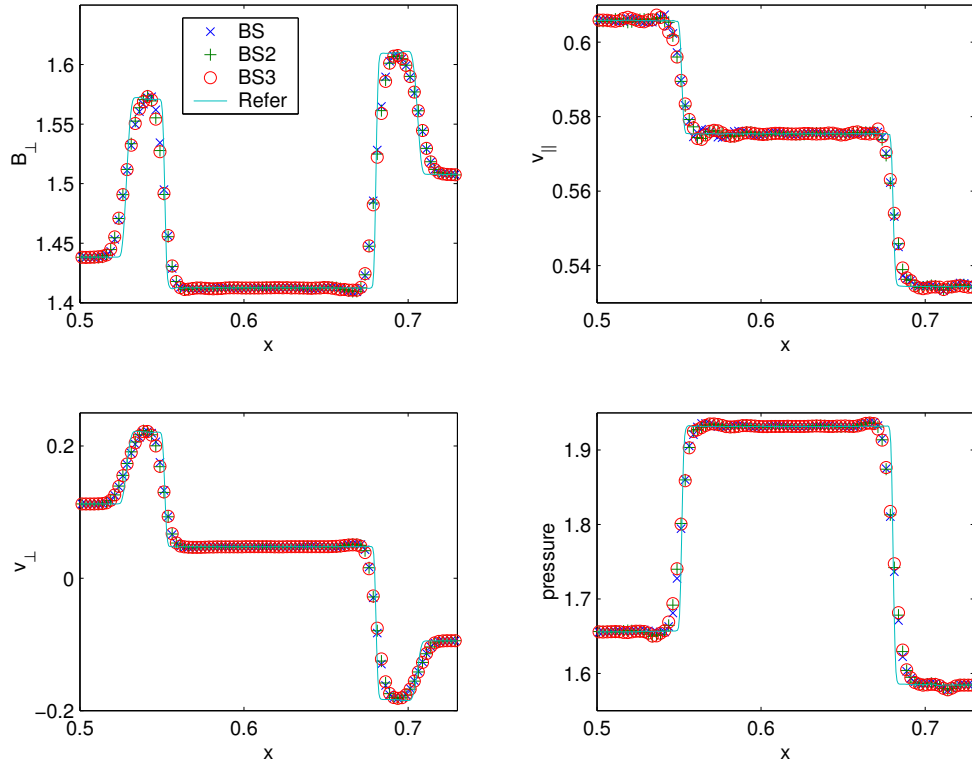


Fig. 4.3.— Results for shock-tube problem ST-2. $\alpha = 45^\circ$. Output is at $t = 0.2/\sqrt{2}$.

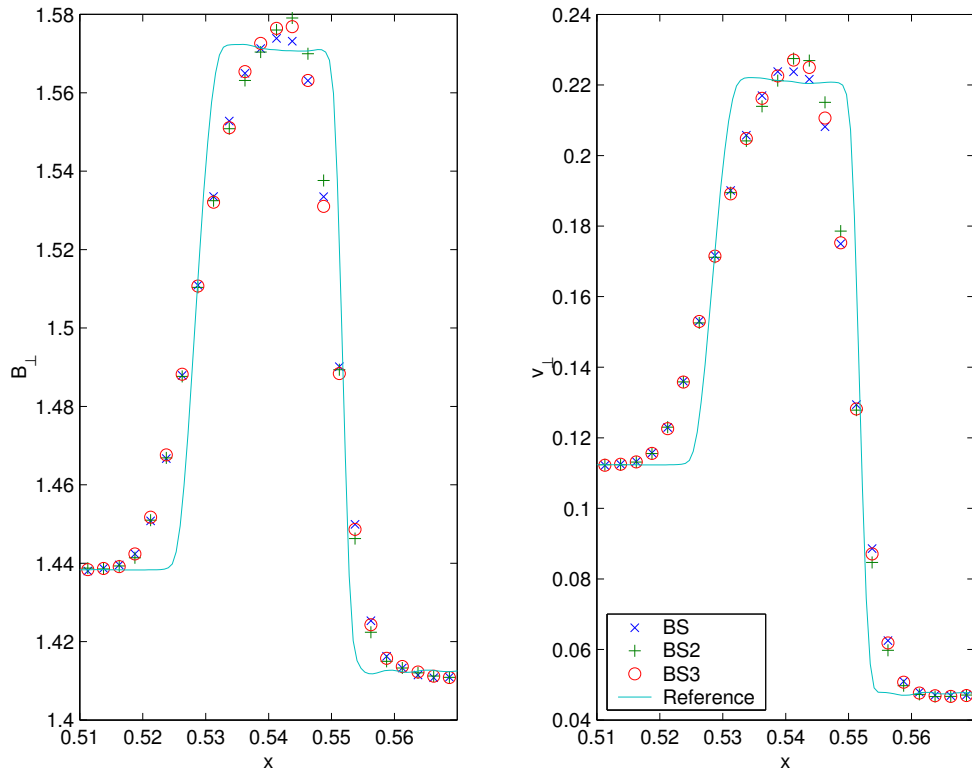


Fig. 4.4.— Results for shock-tube problem ST-2. $\alpha = \tan^{-1} 2$. $\Delta y = 0.5\Delta x$. Output is at $t = 0.2/\sqrt{5}$.

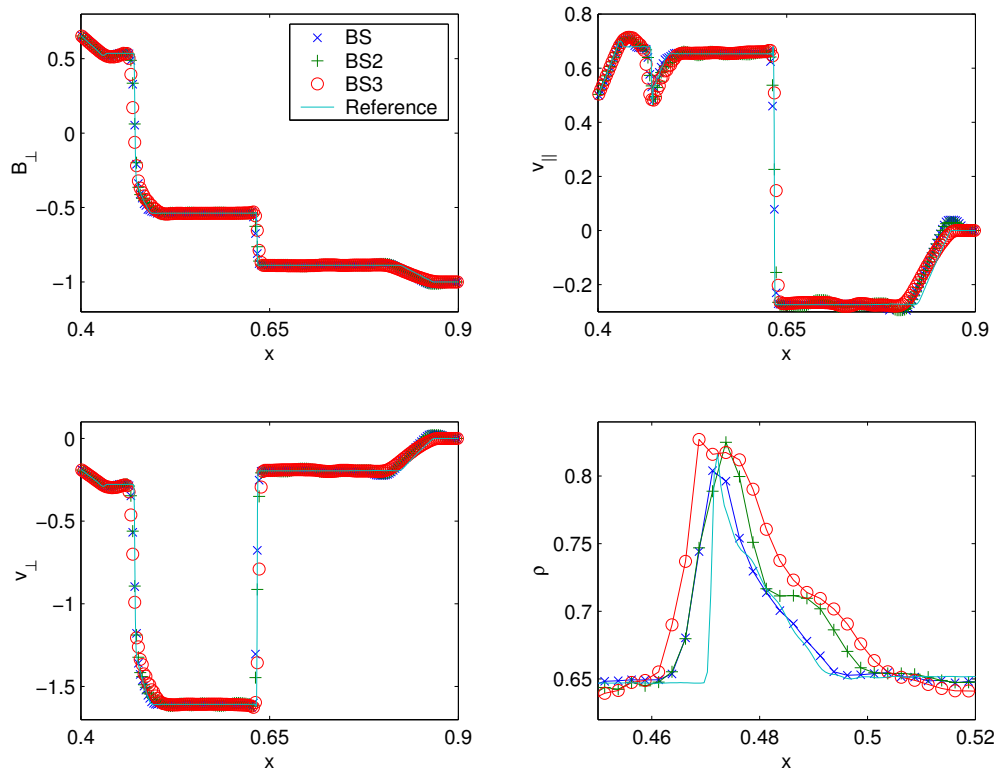


Fig. 4.5.— Results for shock-tube problem ST-3. $\alpha = 45^\circ$. Output is at $t = 0.1/\sqrt{2}$.

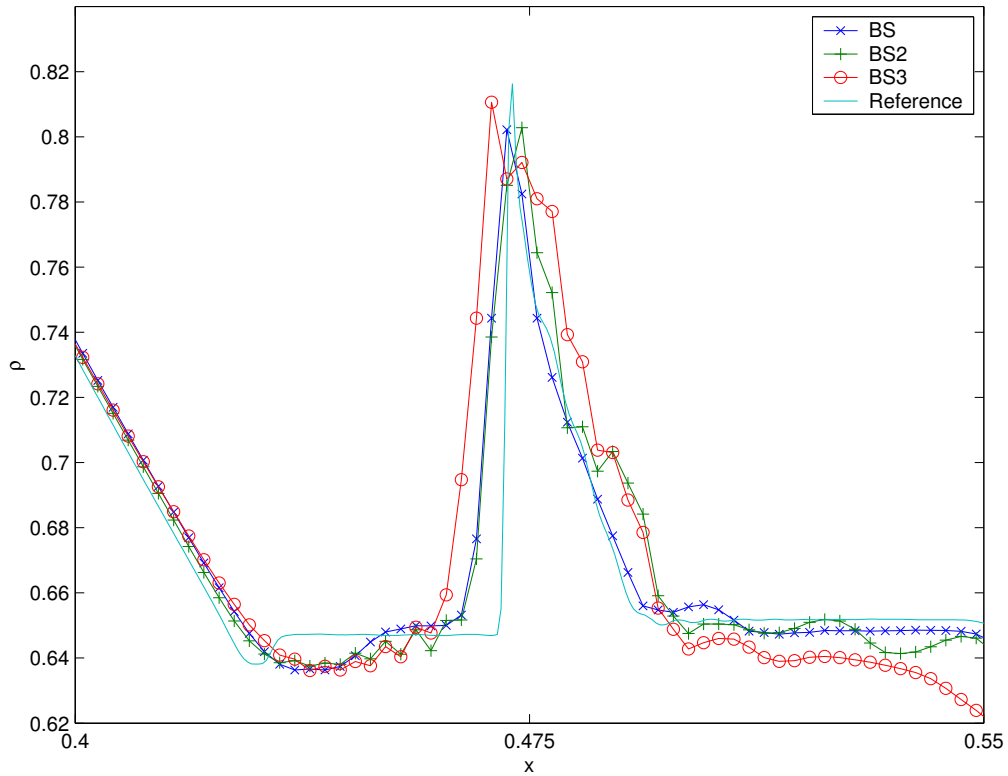


Fig. 4.6.— Results for shock-tube problem ST-3. $\alpha = \tan^{-1} 2$. $\Delta y = 0.5\Delta x$. Output is at $t = 0.1/\sqrt{5}$.

Table 2: Numerical errors for the four rotated shock-tube problems.

α	reconstruction	ST-1	ST-2	ST-3	ST-4
45°	BS	0.0161	0.0143	0.0215	0.0433
	BS2	0.0161	0.0146	0.0235	0.0082
	BS3	0.0259	0.0148	0.0326	0.0081
63.4° $\Delta y = \frac{1}{2}\Delta x$	BS	0.0176	0.0138	0.0219	0.0254
	BS2	0.0177	0.0139	0.0209	0.0131
	BS3	0.0279	0.0140	0.0282	0.0112
63.4° $\Delta y = \Delta x$	BS	0.0339	0.0268	0.0402	0.0388
	BS2	0.0337	0.0260	0.0378	0.0203
	BS3	0.0344	0.0262	0.0367	0.0264

Figs.4.8 and 4.9 show the results for ST-4. Due to a low- β , the flux-CT cannot be run without the energy fix (4) for both angles. It did run for $\alpha = 0$, Therefore we can obtain the reference solution correctly without the energy fix. For both angles, BS generated wrong state for density between the contact and the right slow shock, while BS2 and BS3 obtained almost the same results. We also observed that the wrong state is highly related to the energy deviation from the true energy. Fig.4.7 shows the plot of the energy versus time for $\alpha = 45^\circ$.

We had tested this problem for $\alpha = 0$, for which the numerical magnetic monopole does not exist, with and without energy-fix. BS and BS2 generated exactly the same results while the result for BS3 is slightly different. For all the three schemes, the energy-fix behaves badly even if the upwinding interpolation (3) near the magneto-sonic shock is used. Fig.4.10 shows the results for $\alpha = 0$. Although the results with upwinding interpolation (3) are better than those without, the wrong state is still there. It disappears when (3) is used with $\psi = 1$ throughout the region, which leads to the EMF exactly the same as that for the 1D problem. The reason why the wrong state is almost unnoticeable for BS2 and BS3 for both nonzero α is that the EMF evaluation (2) is closer to the true EMF of the 1D problem than for $\alpha = 0$. As noticed, the results are better in Fig.4.8 for $\alpha = 45^\circ$ than in Fig.4.9 for $\alpha = \tan^{-1} 2$, because (2) is more accurate for $\alpha = 45^\circ$ than for $\alpha = \tan^{-1} 2$.

We believe that the wrong state in the density of ST-4 is due to the energy-fix, because many schemes (e.g. HLLC or hybrid scheme) for ST-4 without using the CT scheme and the divergence-cleaning does not have this wrong state. For the CT schemes, the magnetic field is not obtained directly from the Godunov scheme and the energy-fix is needed to ensure the pressure positivity. Because of the numerical errors in evaluating the EMF, the energy-fix does not preserve the original total energy. This might be one of the disadvantages of the CT method. The numerical magnetic monopole (e.g., for BS with nonzero α) amplifies the effect of the energy-fix. The numerical results also imply that the evaluation of EMF plays

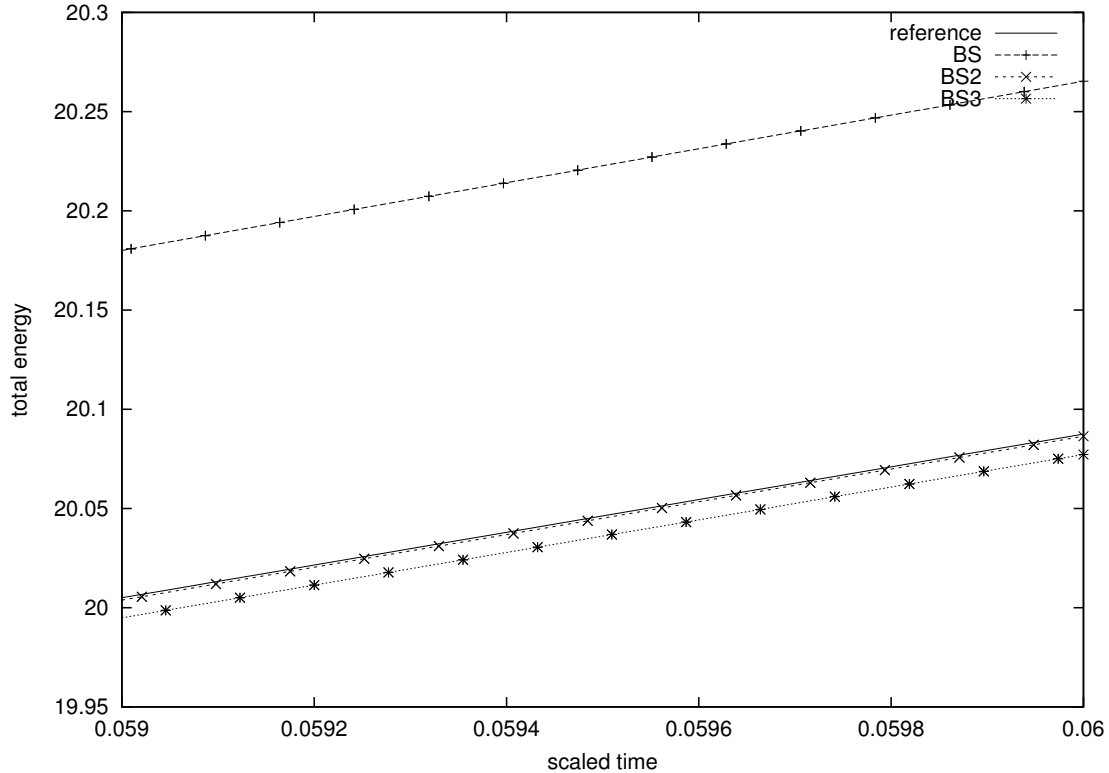


Fig. 4.7.— Results for shock-tube problem ST-4. $\alpha = 45^\circ$. Output is at $t = 0.06$. The energy difference is due to the energy fix (4).

an important role when the energy-fix is used.

The volume-averaging cell-centered values and the divergence-free reconstruction based on \mathbf{b} does improve the results a little bit for both nonzero angles (see the numerical error for BS3 in Table 2), but not good enough to eliminate the need of the energy-fix. For $\alpha = 0$, the results (see Fig.4.10) are even worse for BS3.

4.1.2. Tests for different UCT schemes

Next we test how different UCT schemes compared with the original flux-CT scheme of (Balsara & Spicer 1999). We have tested four schemes, flux-CT of (Balsara & Spicer 1999), modified flux-CT of (Balsara 2003), the transport flux-CT scheme of (Ryu et al. 1998), and the UCT schemes of (Londrillo & Del Zanna 2003). These UCT schemes can be unified by written them as (28) with different smooth parts and dissipative parts. We have described five approaches to evaluate E_{avg} and three approaches to evaluate the dissipative term ϕ . There are 15 possible combinations. However, some combinations are not efficient and will

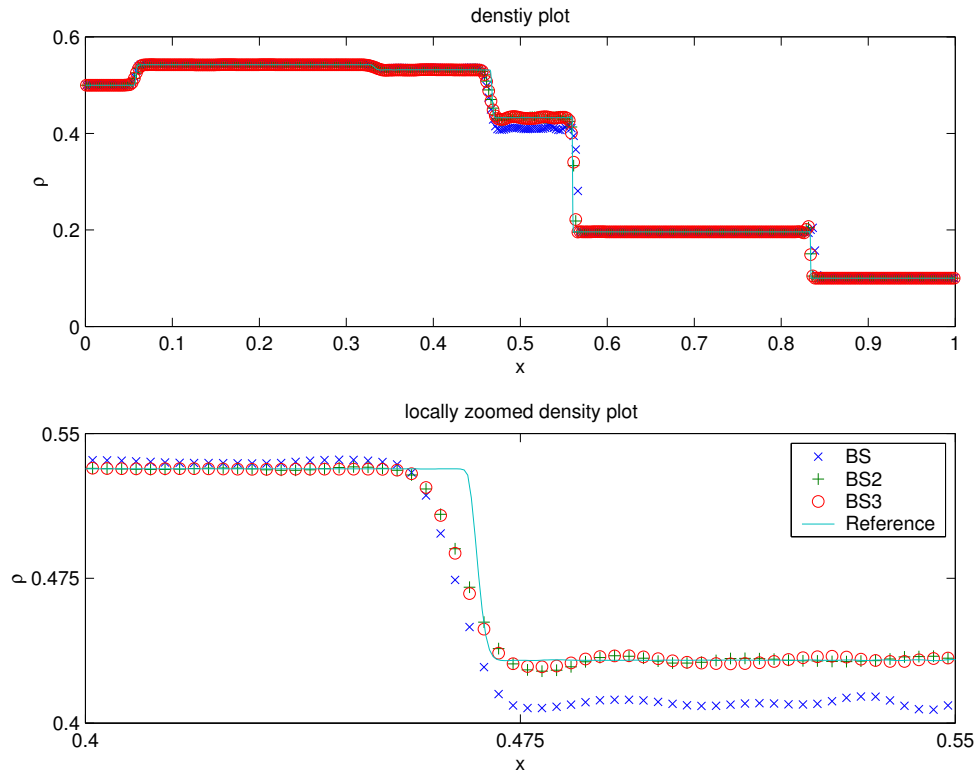


Fig. 4.8.— Results for shock-tube problem ST-4. $\alpha = 45^\circ$. Output is at $t = 0.06/\sqrt{2}$.

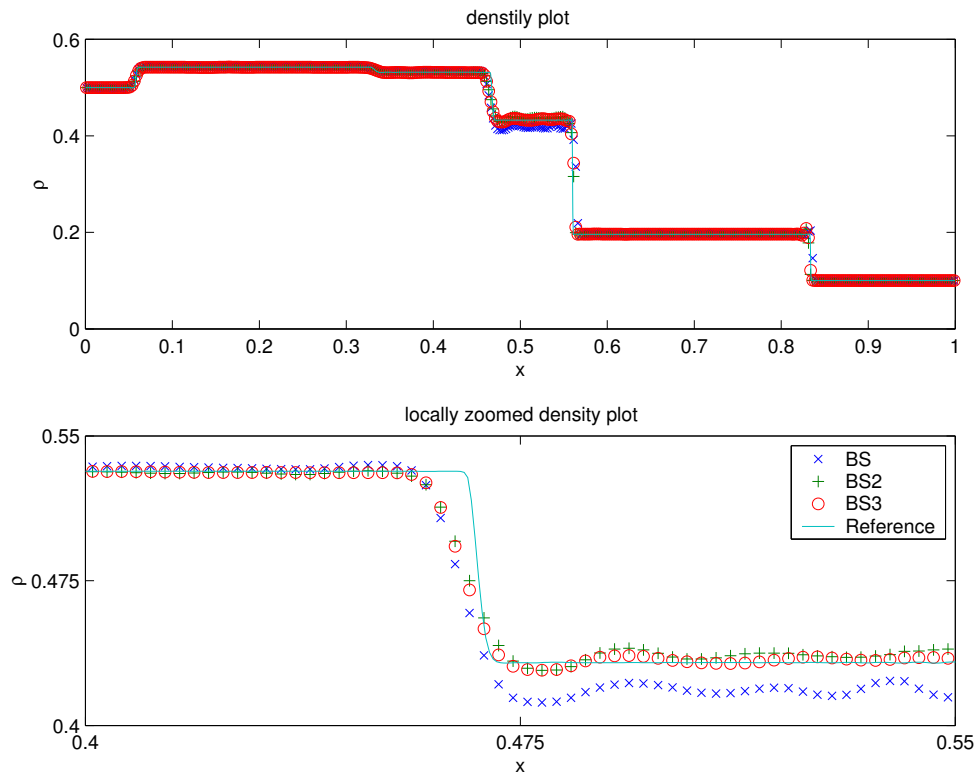


Fig. 4.9.— Results for shock-tube problem ST-4. $\alpha = \tan^{-1} 2$. $\Delta y = 0.5\Delta x$. Output is at $t = 0.06/\sqrt{5}$.

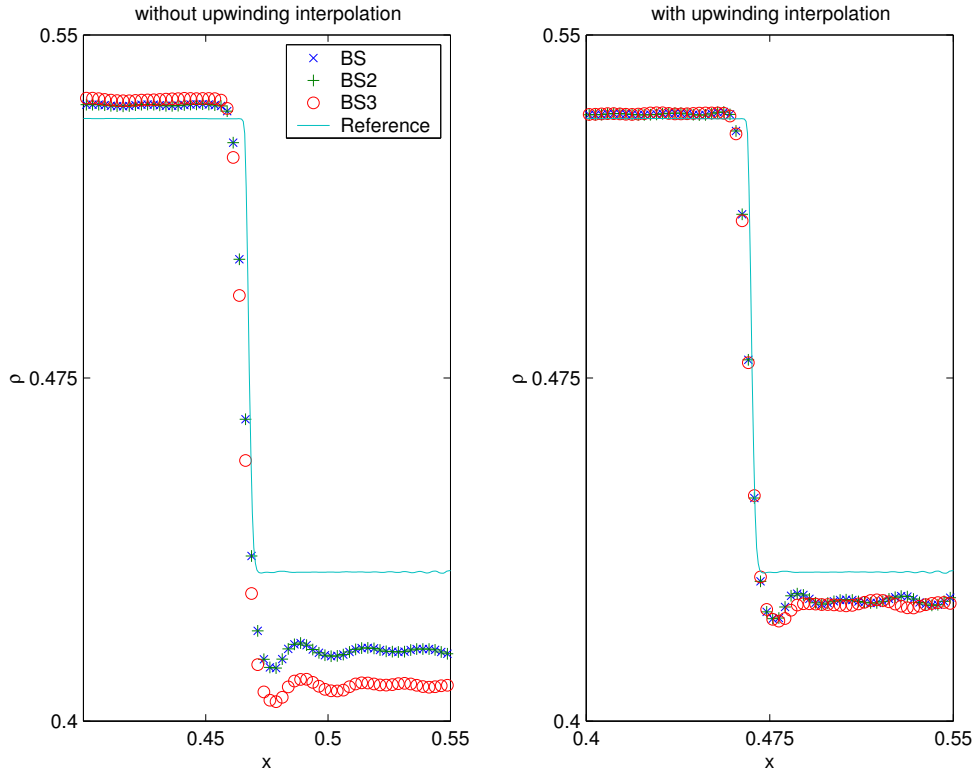


Fig. 4.10.— Results for shock-tube problem ST-4. $\alpha = 0$. Output is at $t = 0.06$. The results for BS and BS2 are exactly the same.

not be tested here.

Since the ϕ term (32) is readily available from the upwind step of a Godunov method, we first test it against different E_{avg} evaluations, among which four of them will be tested: Eq.(22) denoted as E1, Eq.(29) denoted as E2, Eq.(30) denoted as E3, and Eq.(31) denoted as E4.

The results for ST-1 with $\alpha = 45^\circ$ are shown in Fig.4.11. As the previous plots, only the zoomed part of the results is shown. It is clear that the basic flux-CT method (E3 with $c_\phi = 0.25$) is the best among all of the tests (see also the numerical errors in Table 3). Fig.4.12 shows the result of the ST-1 with $\alpha = \tan^{-1} 2$ and $\Delta y = \Delta x$. We do not see too much difference between the results for $c_\phi = 0.5$ and $c_\phi = 0.25$. Again, the basic flux-CT method is one of the best.

One might think that (34), which corresponds to $c_\phi = 0.5$, would be better than (33), which corresponds to $c_\phi = 0.25$, when the shock interface aligns with one of the axes. We tested ST-1 with $\alpha = 0$, which means the shock interface aligns with y -coordinate. The results are shown in Fig.4.13. It seems that (34) is more diffusive for E1, E2, and E3. It is

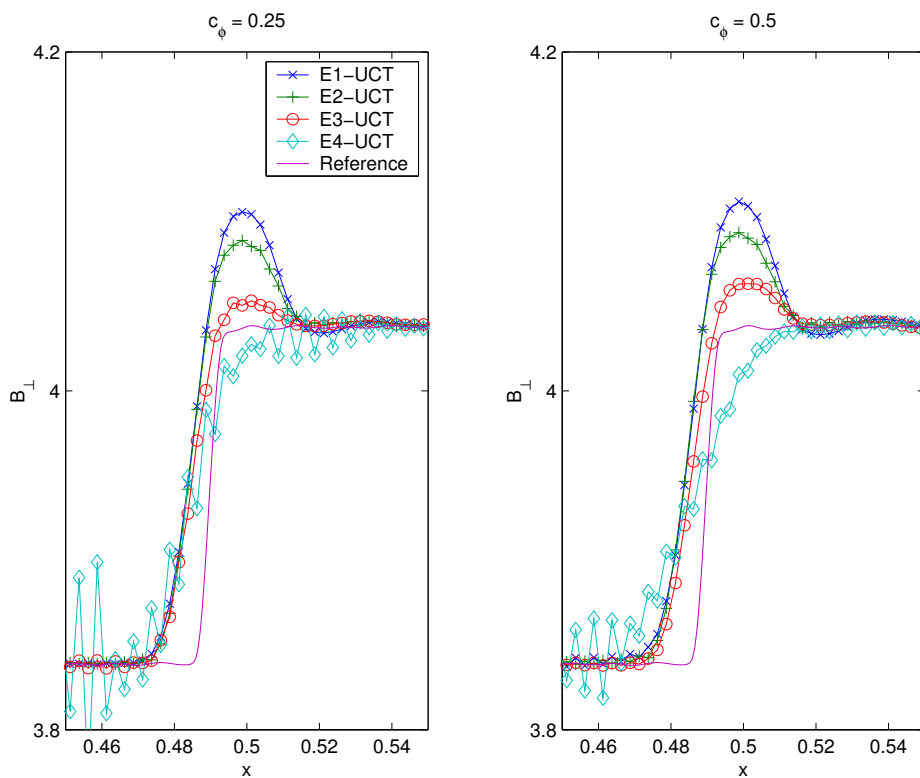


Fig. 4.11.— Results for shock-tube problem ST-1. Only a “zoomed” part from a whole plot is shown. $\alpha = 45^\circ$. Output is at $t = 0.08/\sqrt{2}$.

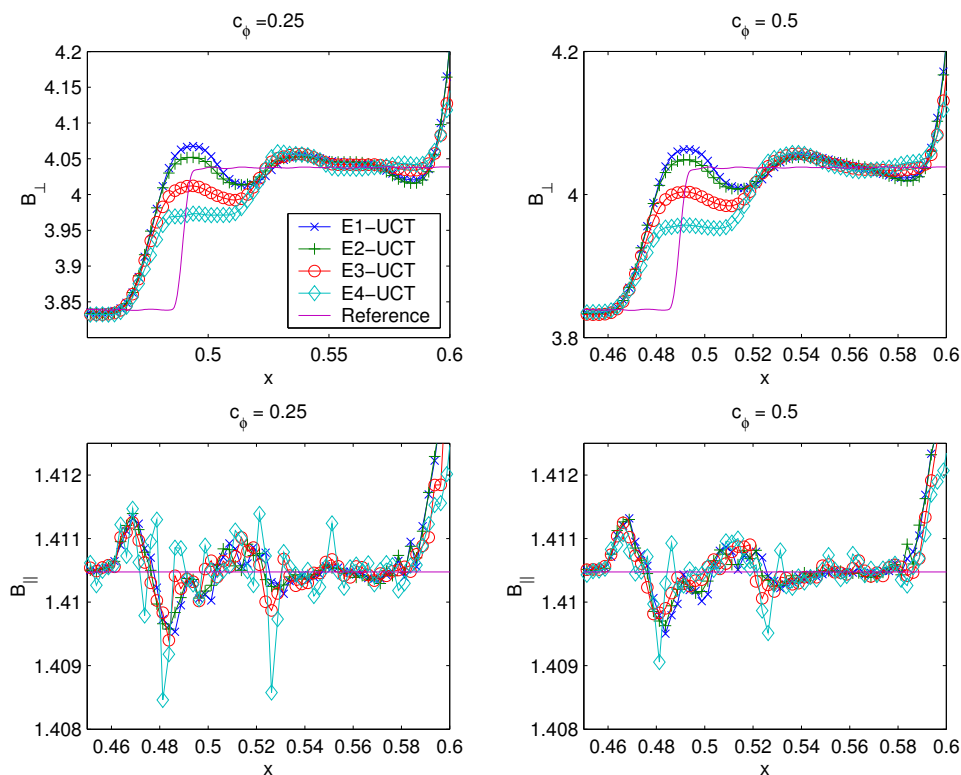


Fig. 4.12.— Results for shock-tube problem ST-1. Only a “zoomed” part from a whole plot is shown. $\alpha = \tan^{-1} 2$. $\Delta x = \Delta y$. Output is at $t = 0.08/\sqrt{5}$.

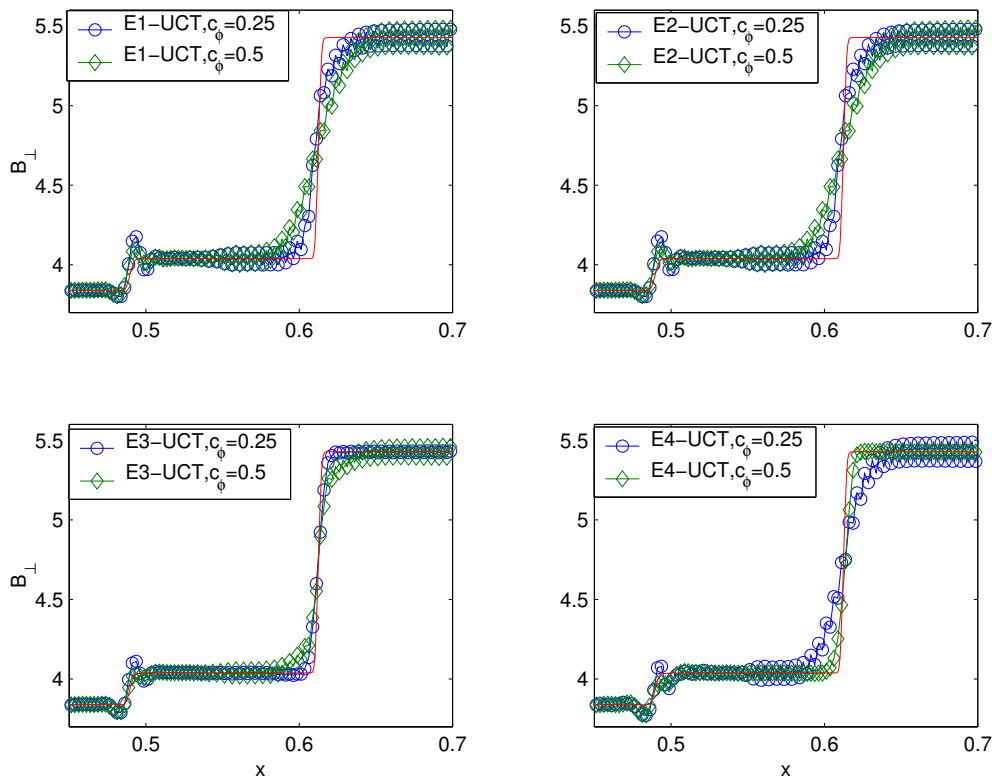


Fig. 4.13.— Results for shock-tube problem ST-1. Only a “zoomed” part from a whole plot is shown. $\alpha = 0$. Output is at $t = 0.08$.

surprised to find that (34) is less diffusive for E4. The result of E3 with $c_\phi = 0.25$ is almost the same as that of E4 with $c_\phi = 0.5$, which is the best among all of the tests.

We also ran the test for the problem ST-2 and found the results were qualitatively the same for different E_{avg} and different c_ϕ evaluations. Fig.4.14 shows the results for ST-3 with $\alpha = \tan^{-1} 2$. E1 resolves the compound structure very well. However there are some oscillations after the compound. The basic flux-CT scheme (E3) also resolves the compound very well, and $c_\phi = 0.5$ improve the results a little bit. E3 with $c_\phi = 0.5$ are the best among all of the tests.

Fig.4.15 shows the results for ST-4 with $\alpha = \tan^{-1} 2$. The energy fix (4) is used. We observed from the plots and the overall error estimates in Table 3 that the E1 and E2 have better results with $c_\phi = 0.5$ than with $c_\phi = 0.25$, and E3 and E4 have better results with $c_\phi = 0.25$ than with $c_\phi = 0.5$. We also tested this problem with Balsara’s modified flux-CT scheme. The original modified flux-CT scheme (Balsara 2003) uses (31) and (35). Here we also tested (35) (denoted as ϕ_3 in the Fig.4.16) combined with other E_{avg} evaluations. The results are shown in Fig.4.16. (35) requires twice as many Riemann solutions as a standard Godunov method. However, the results are worse than those for the original flux-CT method.

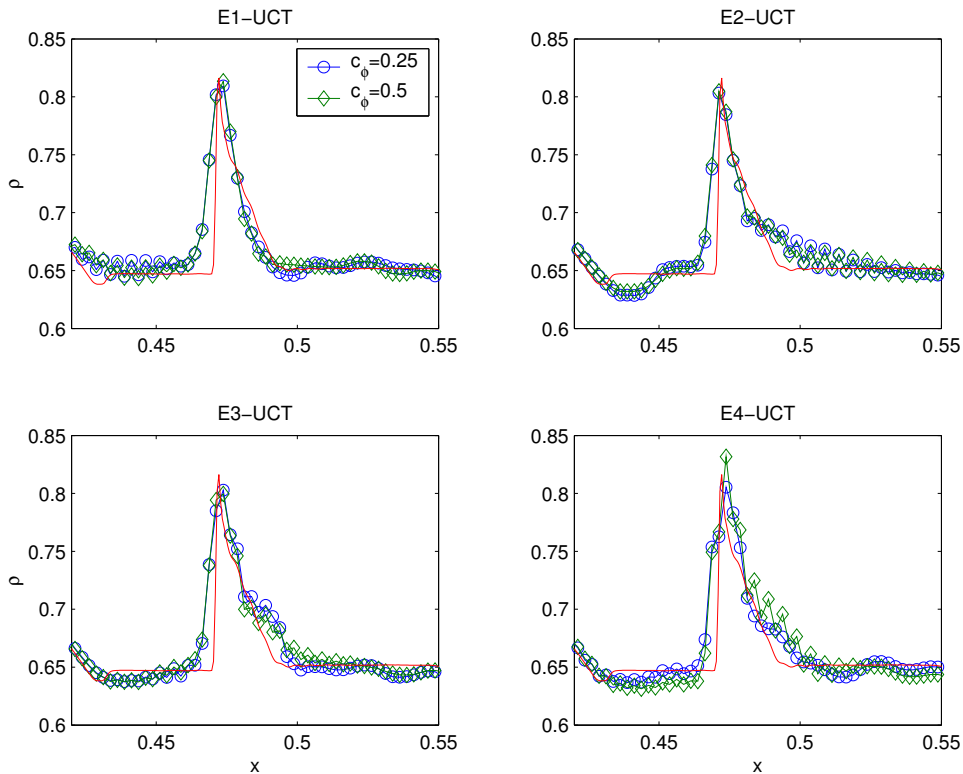


Fig. 4.14.— Results for shock-tube problem ST-3. Only the compound structure is shown. $\alpha = \tan^{-1} 2$. $\Delta y = 0.5\Delta x$. Output is at $t = 0.1/\sqrt{5}$.

We also tested it for other shock-tube problems and found no improvement at all.

For a clear comparison, the numerical errors defined as (36) are listed in Table 3.

4.2. The Blast problem

This test problem was first introduced in Balsara and Spicer (Balsara & Spicer 1999). It was about a spherical strong fast magneto-sonic shock propagates through a low- β ($\beta = 0.000251$) ambient plasma. It was used as an example in (Balsara 2003) to show the advantages of the divergence-free reconstruction (7) and (8). We tested this problem to compare different UCT schemes and reconstructions. The set-up of the problem is exactly the same described in (Balsara & Spicer 1999). 200×200 grid is used. The final time is 0.01. The results are shown in Fig.4.17.

It was pointed out in (Balsara 2003) that the divergence-free reconstruction (BS2 or BS3) helped overcome some of the problems that arise in maintaining the positivity of the pressure variable in low- β simulation like this one. However, we find the energy-fix (4) is

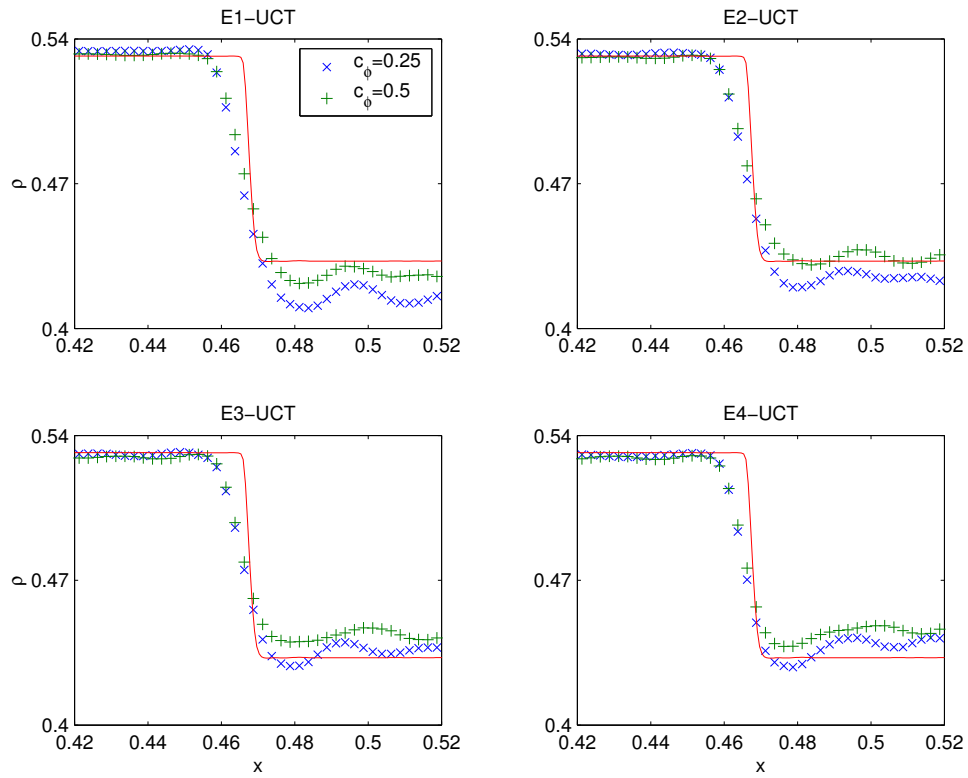


Fig. 4.15.— Results for shock-tube problem ST-4. $\alpha = \tan^{-1} 2$. Output is at $t = 0.06/\sqrt{5}$.

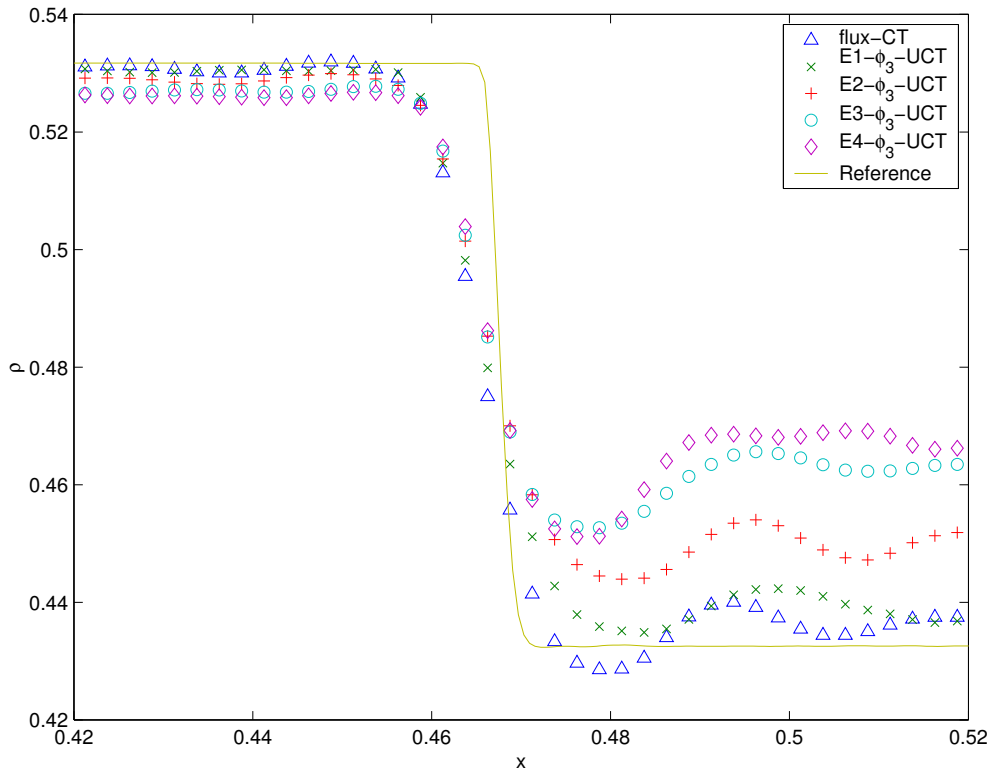


Fig. 4.16.— Results for shock-tube problem ST-4. $\alpha = \tan^{-1} 2$. $\Delta y = 0.5\Delta x$. Output is at $t = 0.06/\sqrt{5}$.

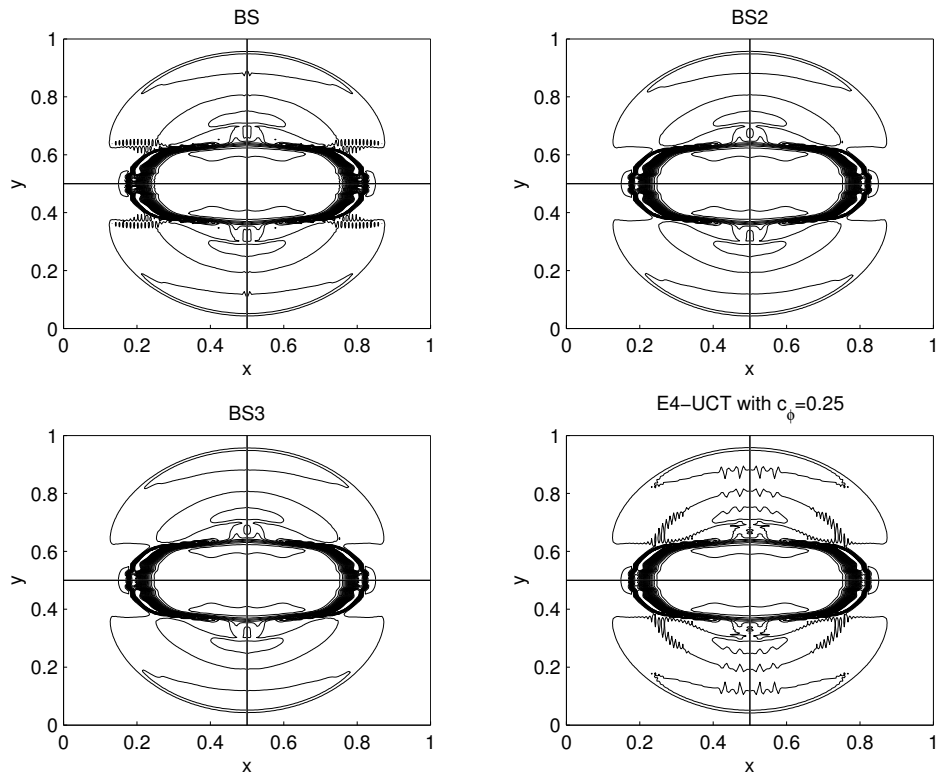


Fig. 4.17.— Results for blast problem. 30 contours between 0.1 and 4.0 are used.

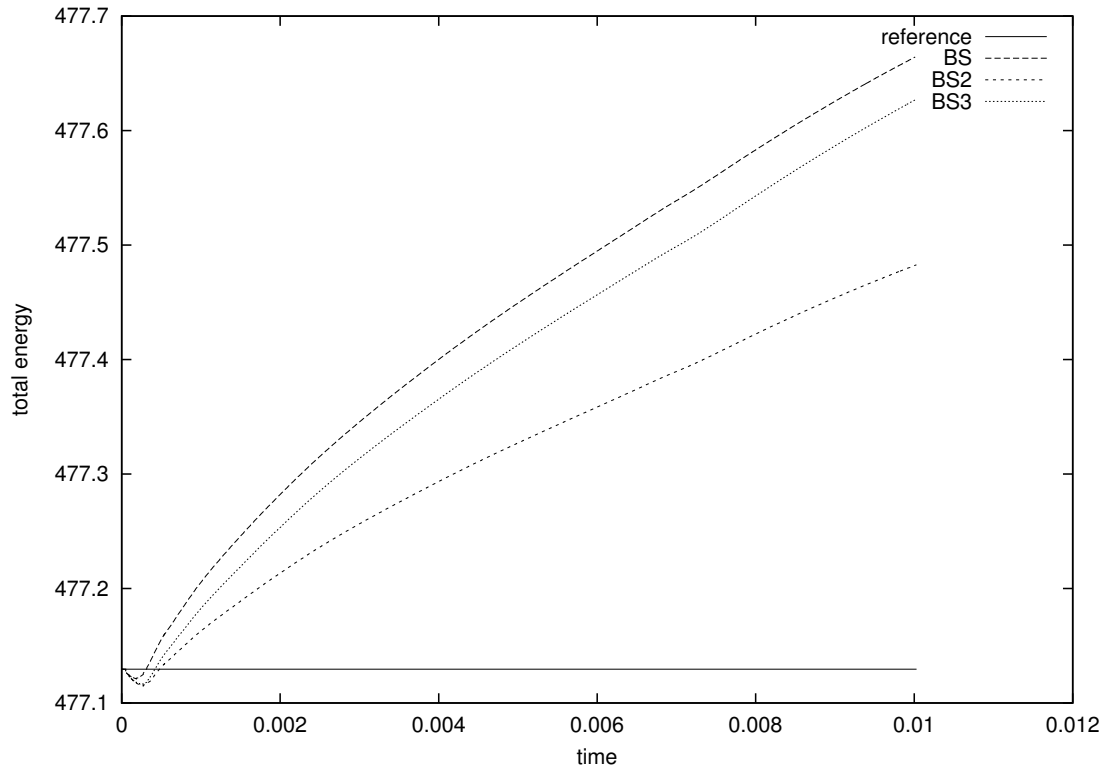


Fig. 4.18.— Total energy versus time for blast problem.

Table 3: Numerical errors of the different UCT schemes for the four rotated shock-tube problems.

c_ϕ	EMF	ST-1, $\alpha=45^\circ$	ST-1*, $\alpha=63.4^\circ$	ST-1, $\alpha=0$	ST-3	ST-4
0.25	E1	0.0290	0.0355	0.0473	0.0232	0.0331
	E2	0.0205	0.0352	0.0473	0.0241	0.0157
	E3	0.0177	0.0336	0.0141	0.0209	0.0131
	E4	0.0191	0.0341	0.0673	0.0198	0.0170
0.5	E1	0.0360	0.0361	0.0573	0.0215	0.0123
	E2	0.0205	0.0357	0.0573	0.0216	0.0143
	E3	0.0178	0.0349	0.0322	0.0189	0.0250
	E4	0.0179	0.0353	0.0132	0.0232	0.0269

ST-1* represents $\Delta y = \Delta x$ case.

still needed despite the divergence-free reconstruction. We believe it is because of the energy fix, *not the divergence-free reconstruction*, the positivity of the pressure is maintained. It is clear in Fig.4.17 that both divergence free reconstructions indeed improve the results of the original flux-CT scheme, and there is no qualitative difference between the results of BS2 and BS3. We also tested this problem by using different UCT schemes. All of them failed due to the negative pressure when $c_\phi = 0.5$ is used. With $c_\phi = 0.25$, only E3, which is also BS scheme, and E4 worked with CFL number of 0.7 (the result is shown in Fig.4.17). E1 and E2 worked with CFL=0.4 and their results (not shown here) are almost identical.

Fig.4.18 shows the total energy deviation. Since the periodic boundary conditions are used, the total energy should be conserved physically. However, due to the energy-fix, the total energy is not conserved. Fig.4.18 shows that the BS2 reconstruction is the best in preserving energy for this problem. We have solved this problem with an eight-wave model of (Janhunen 2000), which adds the divergence source term only to the induction equations. The solution has a lot of noise (see Fig.4.19) due to the numerical magnetic monopole, despite that the energy is conserved. We also tested another approach which sets the pressure to a minimal value once it becomes negative. The divergence-free condition can be preserved by the flux-CT method and the energy is also preserved by the Godunov method. However, the results are not very good (see Fig.4.19).

Some might think that the energy conservation would be better if the energy fix is applied only when the pressure becomes negative. We tested it for both the ST-4 and the blast problems. It turns out that the results are even worse. So it is not recommended.

We have tested the schemes with other 2D examples, such as the rotor problem of (Balsara & Spicer 1999) and shock-cloud interaction problem of (Dai & Woodward 1998). There is no noticeable difference between the results of all the CT schemes. The results of the modified flux-CT are no better than those of the original flux-CT scheme.

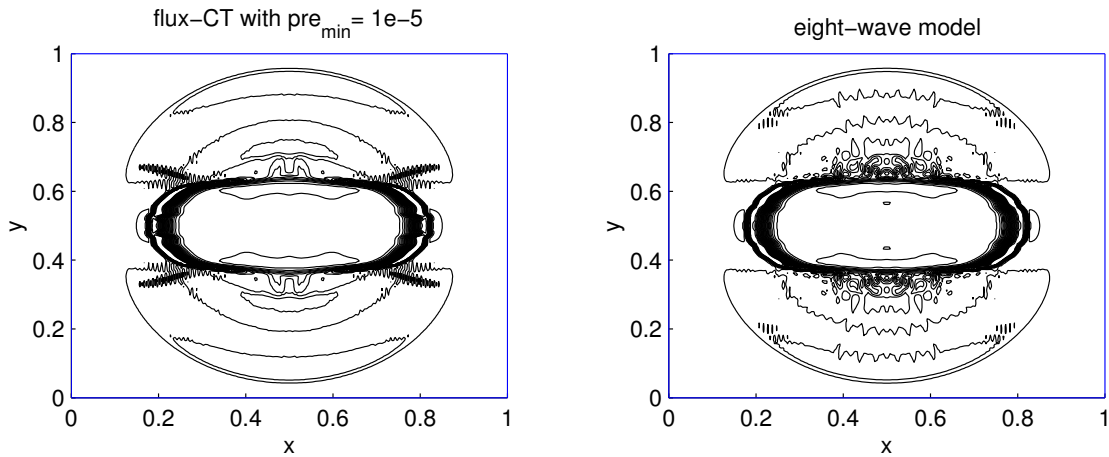


Fig. 4.19.— Results for blast problem. 30 contours between 0.1 and 4.0 are used.

5. Conclusions

After compared the results, we obtain the following observations for the UCT schemes:

- The more complex divergence-free reconstruction of (Balsara 2000) is no better than the simple divergence-free reconstruction of (Londrillo & Del Zanna 2003) in most cases.
- Only when the energy fix is used for low- β plasma, the divergence-free reconstruction is better than the standard limited reconstruction of the cell-centered values.
- The flux-CT method is one of the best among all of the UCT methods.
- Despite more computations, the more complex modified flux-CT scheme of (Balsara 2003) is no better than the original flux-CT scheme of (Balsara & Spicer 1999).
- The arithmetic averaging of the face-interface values to obtain the cell-centered values for magnetic field is as good as the more complex volume-average cell-centered values for the second order method.

It is important to notice that the divergence-free reconstruction is not needed for CT scheme for most of the problems, because the dimensional splitting solvers, which have been widely used and more efficient, cannot have this property.

For low- β plasma, the CT methods may result in a negative pressure. If the energy-fix is used, the overall conservation will be destroyed and wrong state could be generated. This is one of the disadvantages of the CT methods. We are exploring to construct a CT method that does not need the energy-fix.

We should point out that our test is only for the second order scheme with constrained transport for magnetic field. It may not be valid for other higher order schemes. However, constructing a higher order scheme requires a higher order reconstruction for the magnetic fields. The divergence-free reconstruction described in (Balsara 2000) and (Londrillo & Del Zanna 2003) is of only the second order accuracy.

Although our tests and descriptions are based on Roe’s type Riemann solver, We also tested the examples using other Riemann solvers, such as HLL, HLLC and hybrid (combined Roe’s and HLL) Riemann solver, and we have drawn the same conclusions.

Although the HLL scheme(Janhunen 2000) can preserve the positivity, this property is lost when HLL is combined with any CT scheme. Therefore, for the low- β plasma, the energy fix (4) is still needed.

REFERENCES

- D. S. Balsara and D. S. Spicer, A staggered mesh algorithm using high order Godunov fluxes to ensure solenoidal magnetic fields in magnetohydrodynamics simulations, *J. Comput. Phys.* 149 (1999), 270-292.
- D. S. Balsara, Total variation diminishing scheme for adiabatic and isothermal magnetohydrodynamics, *ApJS*, 116 (1998), 133.
- D. S. Balsara, Divergence-free adaptive mesh refinement for magnetohydrodynamics, *J. Comput. Phys.*, 174 (2001), 614-648.
- D. S. Balsara, Second order accurate schemes for magnetohydrodynamics with divergence-free reconstruction, astro-ph/0308249, (2003).
- J. U. Brackbill and D. C. Barnes, The effect of nonzero $\nabla \cdot B$ on the numerical solution of the magnetohydrodynamic equations, *J. Comput. Phys.*, 35 (1980), 426.
- M. Brio and C. C. Wu, An upwinding differencing schemes for the equations for ideal Magnetohydrodynamics, *J. Comput. Phys.*, 75 (1988), 400.
- W. Dai and P. R. Woodward, Extension of piecewise parabolic method (PPM) to multidimensional magnetohydrodynamics, *J. Comput. Phys.*, (111 (1994), 354.
- W. Dai and P. R. Woodward, A simple finite difference scheme for multidimensional magnetohydrodynamics, *J. Comput. Phys.* 142 (1998), 331-369.
- C. R. DeVore, Flux corrected transport techniques for multidimensional compressible magnetohydrodynamics, *J. Comput. Phys.*, 92 (1992), 142.

- A. Dedner, F. Kemm, D. Kroner, C. D. Munz, T. Schnitzer and M. Wesenberg, Hyperbolic divergence-cleaning for the MHD equations, *J. Comput. Phys.*, 175 (2002), 645.
- C. R. Evans and J. F. Hawley, Simulation of magnetohydrodynamic flows: A constrained transport method, *Astrophys. J.* 332 (1989), 659.
- S. A. E. G. Falle, Rarefaction shocks, shock errors, and low order of accuracy in ZEUS, *ApJ*, 577 (2002), 123-126.
- P. Janhunen, A positive conservative method for magnetohydrodynamics based on HLL and Roe methods, *J. Comput. Phys.* 160 (2000), 649.
- G. S. Jiang and C.-C. Wu, A high-order WENO finite difference scheme for the equations of ideal Magnetohydrodynamics, *J. Comput. Phys.*, 150 (1999) 561-594.
- P. Londrillo and L. Del Zanna, High-order upwinding schemes for multidimensional magnetohydrodynamics, *Astrophysics, J.* 530 (2000), 508.
- P. Londrillo and L. Del Zanna, On the divergence-free condition in Godunov-type schemes for ideal magnetohydrodynamics: the upwind constrained transport method, to appear in JCP, 2003.
- S. Li and H. Li, A modern code for solving magnetohydrodynamics or hydrodynamic equations, Technical Report, Los Alamos National Laboratory, 2003.
- K. G. Powell, *An approximate Riemann solver for MHD (that actually works in more than one dimension)*, Technical Report N0. 94-24, (ICASE, Langley VA, 19994).
- K. G. Powell, P. L. Roe, T. J. Linde, T. I. Gombosi, and D. L. DeZeeuw, A solution-adaptive upwinding scheme for ideal magnetohydrodynamics, *J. Compt. Phys.*, 154 (1999), 284.
- P. L. Roe and D. S. Balsara, Notes on the eigen-system of magnetohydrodynamics, *SIAM J. Appl. Math.*, 56 (1996), 57.
- D. Ryu and T. W. Jones, Numerical magnetohydrodynamics in astrophysics: algorithm and tests for one-dimensional flow. *ApJ*, 442 (1995), 228-258.
- D. Ryu, F. Miniati, T. W. Jones, and A. Frank, A divergence-free upwinding code for multi-dimensional MHD flows, *Astrophysics. J.*, 509 (1998), 244-255.
- Gabor Tóth, The $\nabla \cdot B = 0$ constraint in shock-capturing magnetohydrodynamics codes, *J. Comp. Phys.*, 161 (2000), 605-652.
- M. Wesenberg, Efficient MHD Riemann solvers for simulations on unstructured triangular grids, *J. Numer. Math.*, 10 (2002), 37-71.

- A L. Zachary, A. Malagoli, and P. Colella, A higher-order Godunov method for multidimensional ideal magnetohydrodynamics, *SIAM J. Sci. Comput.*, 15 (1994), 263.
- K. S. Yee, Numerical solution of initial boundary value problems involving Maxwell's equation in an isotropic media, *IEEE Trans. Antenna Propagation* AP-14 (1966), 302